February 1986
LU TP 86-1

Initial State Radiation Effects on W and Jet Production

Mats Bengtsson, Torbjörn Sjöstrand, Maria van Zijl
Department of Theoretical Physics,
University of Lund, Sölvegatan 14A,
S-223 62 Lund, Sweden

Abstract:

A model for initial state parton showers, previously presented briefly, is here discussed in more detail. Experimentally, the transverse momentum spectrum of W and Z, and the associated jet activity, are the most obvious signals for initial state radiation. We show that these effects are well described by our model, compare with analytic calculations, and discuss the uncertainty due to various open issues in the description of initial state radiation. Other subjects studied include radiation effects on jet cross sections and the transverse energy flow. Results are presented for a wide range of CM energies.

1. Introduction

Bremsstrahlung phenomena appear inevitably in a field theory description of high energy interactions. In QED, scatterings between charged particles are accompanied by the emission of photons. In QCD, the candidate theory of strong interactions, scatterings between coloured partons result in the production of additional partons. Because of the large strong coupling constant α_s (as compared with α_{em}), and because gluons carry colour charge (whereas photons are electrically neutral), radiation effects are normally more important in QCD than in QED.

In general, it is not possible to subdivide bremsstrahlung effects into initial state and final state radiation, because of the presence of interference terms. In this respect, W and Z production at hadron colliders take on a special rôle: in processes like $u\bar{d} \to W^+ \to e^+\nu_e$ or $u\bar{u} \to Z^0 \to e^+e^-$ the final state does not contain any colour charges. All (QCD) bremsstrahlung effects are therefore attributable to initial state radiation. Observations by the UA1 [1] and UA2 [2] collaborations show that these bosons are produced, not with the typical "intrinsic k_T" of a few hundred MeV, but rather with several GeV of transverse momentum. In addition, the transverse momentum balance is carried mostly by jets at fairly central rapidities, rather than e.g. by the beam remnants. Both observations are in agreement with QCD expectations.

Whereas the effects of initial state radiation are particularly transparent to observe in the case of W and Z production, they are not expected to be any less important for ordinary high-p_T events. In this paper we will discuss one specific approach to the problem of understanding these effects, that of Monte Carlo simulation of initial state parton showers. This technique is more powerful, but also more limited, than conventional analytic approaches. More powerful, since it allows a more detailed description of the complete event structure, with direct reference to experimental consequences. More limited, since the universal characteristics of initial state radiation are emphazised at the expense of the process-specific details. Therefore Monte Carlo and analytic studies should be considered as complementary rather than competing.

Within the framework of perturbation theory, radiation effects appear as higher order corrections to the basic process. The first order corrections contain terms corresponding to the emission of one additional parton, as well as virtual corrections to the lowest-order graph. Calculations to higher orders are increasingly difficult, and only in the case of e^+e^- annihilation have, so far, full second (nontrivial) order matrix elements been presented [3]. This severely limits the possibility to study effects characterized by the emission of many partons. For the W p_T spectrum, exponentiation of lower order results have been used to sum up multiple emission effects, but such methods could not be used e.g. to describe detailed properties of the emitted partons.

In the approach adopted in this paper, two major approximations are necessary. The first involves a separation of initial state and final state radiation. As we noted above, a process like $u\bar{u} \to Z^0 \to e^+e^-$ can only contain initial state radiation, because the final state does not contain any colour charges. In $e^+e^- \to Z^0 \to d\bar{d}$ the reverse applies: only final state radiation is possible. For a process with colour charges in both the initial and the final state, like $u\bar{u} \to Z^0 \to d\bar{d}$, our standard approximation will be to consider initial state radiation as if the final state did not contain any colour charges, and vice versa for final state radiation.

Bremsstrahlung close to the directions of the two incoming partons, u and $\bar{u}$ above, is obviously dominated by the collinear divergences from initial state radiation graphs, and correspondingly final state radiation dominates close to the directions of the two outgoing partons, d and $\bar{d}$ above. The interference terms are most important for the rate of lower-energy partons emitted at large, or at least comparable, angles with respect to both the initial and the final partons. We therefore expect that the dropping of the interference terms should be less important for the overall picture.

With the recipe above for separating initial and final state radiation, it would still have been possible to calculate matrix elements to higher and higher orders. Our second approximation is to adopt a parton shower approach to initial state radiation and final state radiation separately. In parton showers, the leading order formulae for the basic parton branchings $q \to qg$, $g \to gg$ and $g \to q\bar{q}$ are applied repeatedly, to give a multiparton configuration. This description is process-independent, in the sense that only the common singularity structure is included in the branching rules, rather than the full structure of the process-dependent matrix elements. Because of these collinear

approximations, parton showers are less reliable for hard parton emission at large angles than for the small-angle behaviour.

Despite the appearance of the same basic branchings, the structure of an initial and a final state shower is rather different. The latter shower is timelike: all partons have $m^2 \geqslant 0$. The parton that emerges from the hard interaction has the largest mass, and then successively branches into partons with smaller and smaller masses and energies, until eventually all partons end up on mass shell (modulo confinement effects). The initial state shower, on the other hand, is spacelike: at least one of the partons in the cascade has a virtuality $Q^2 = -m^2 > 0$. As the shower evolves, the energy is again split between more and more partons, but the virtuality Q^2 is increasing.

For the timelike parton showers of final state radiation, a number of algorithms have been developed and studied over the years [4-6]. Two of these have been implemented by us [7] and are used below, the "conventional" scheme of Kajantie and Pietarinen [5] and the "coherent" one of Marchesini and Webber [6]. The latter correctly takes into account a number of interference effects [8,9], while the former does not, but for our applications differences are small.

The field of initial state parton showers has been considerably less well studied. Two "forward" evolution shemes have been developed, one by Odorico [10] and one by Field, Fox, Kelly and Shatz [11]. In this approach, the shower evolution is followed from initial partons, chosen according to the structure functions at some small virtuality Q_0^2, up towards the momentum transfer scale Q^2 of the hard interaction, i.e. naively forward in time. In [12] we presented a "backward" evolution scheme. Here the hard interaction is selected first, using Q^2-evolved structure functions, and then the preceding branchings are reconstructed step by step in falling Q^2 sequence, back towards the shower initiators at the low Q_0^2 scale. This approach contains a number of distinct advantages, that will be discussed below. Another such scheme has been presented by Gottschalk [13], in a formulation which allows the study of some aspects that are not easily accessible with our approach, unfortunately at the price of a greatly increased complexity (both papers [13] contain a number of significant errors, which have since been found and corrected).

In section 2 our scheme is presented in more detail. The Collider W production data are used as a first check in section 3, and comparisons are also presented with analytic calculations, where available. A number of suggestions

are made for further experimental studies that could be of interest. The significantly more complex field of high-p_T jet production is considered in section 4. Some general conclusions are presented in section 5.

2. The Model

The basics of our model were described in [12]. We will here repeat the relevant formulae, present additional details and discuss open issues. In section 2.1 we introduce some terminology and, at the same time, try to provide an intuitive picture of spacelike shower evolution. The details of longitudinal and transverse evolution are presented in 2.2 and 2.3, respectively. Some final comments on various aspects are collected in 2.4.

2.1. Preliminaries

A fast hadron may be viewed as a cloud of quasireal partons. At each instant, an individual parton can initiate a virtual cascade, branching into a number of partons. This cascade can be described in terms of a tree-like structure, as composed of many branchings $a \to bc$, i.e. $q \to qg$, $g \to gg$ or $g \to q\bar{q}$. Each branching $a \to bc$ involves some relative transverse momentum between the partons b and c. In a language where four-momentum is conserved at each vertex, this implies that at least one of the b and c partons must have a spacelike virtuality, $m^2 < 0$. Since the partons are not on mass shell, the cascade only lives a finite time before reassembling, with those parts of the cascade that are most off mass-shell living the shortest time.

A hard scattering, e.g. in deep inelastic leptoproduction, will probe the hadron at a given instant. The probe, the virtual photon in the leptoproduction case, is able to resolve fluctuations in the hadron up to the Q^2 scale of the hard scattering. Thus probes at different Q^2 values will seem to see different parton compositions in the hadron. This is expressed by the Altarelli-Parisi (AP) evolution equations [14]

$$\frac{df_b(x,t)}{dt} = \frac{\alpha_s(t)}{2\pi} \sum_a \int \frac{dx'}{x'} f_a(x',t)\, P_{a\to bc}\left(\frac{x}{x'}\right) \tag{1}$$

Here the $f_i(x,t)$ are the parton structure functions, expressing the probability of finding a parton i carrying the fraction x of the total hadron momentum if the hadron is probed at a virtuality Q^2. The variable t is here

and in the following used as shorthand for $\ln(Q^2/\Lambda^2)$, with Λ the QCD scale parameter. Thus the first order strong coupling constant is

$$\alpha_s(Q^2) = \frac{12\pi}{(33-2n_f)\ \ln(Q^2/\Lambda^2)} = \frac{12\pi}{(33-2n_f)\ t} = \alpha_s(t) \tag{2}$$

where n_f is the number of flavours that can be probed at that scale, usually 4 or 5. Finally, the AP splitting kernels $P_{a\to bc}(z)$ are given by

$$\begin{aligned} P_{q\to qg}(z) &= \frac{4}{3}\,\frac{1+z^2}{1-z} \\ P_{g\to gg}(z) &= 6\,\frac{(1-z(1-z))^2}{z(1-z)} \\ P_{g\to q\bar{q}}(z) &= \frac{1}{2}\,(z^2+(1-z)^2) \end{aligned} \tag{3}$$

The absolute form of structure functions can not be predicted in perturbative QCD. Rather, experimental data are used to find parametrized structure function sets, with the Q^2 dependence in accordance with the AP equations. In this paper we will use Eichten-Hinchliffe-Lane-Quigg sets 1 and 2 (EHLQ1, EHLQ2) [15], Duke-Owens sets 1 and 2 (DO1, DO2) [16] and Glück-Hoffmann-Reya (GHR) [17]. In these different parametrizations somewhat different assumptions are made, e.g. about the shape of the gluon structure function at small Q^2 and, more importantly, about the Λ values to use; in the parametrizations above Λ = 0.2, 0.29, 0.2, 0.4 and 0.4 GeV, respectively.

If a hard interaction scatters a parton out of the incoming hadron, the "coherence" [8] of the cascade it belongs to is broken: the partons can no longer reassemble completely back to the cascade-initiating parton. In this semiclassical picture, the "main chain" (see Fig. 1) of consecutive branchings that lead directly from the initiating parton to the scattered parton can no longer disappear, whereas fluctuations on "side branches" to this chain may still reassemble. A convenient description is obtained by assigning a spacelike virtuality to the partons on the main chain, in such a way that the partons on the side branches may be on mass shell. Since the momentum transfer of the hard scattering can put the scattered parton on mass shell (or even give it a timelike virtuality, so it can start a final state shower), one is then guaranteed that no partons have a spacelike virtuality in the final state (again neglecting confinement effects). If no hard scattering had taken place, the virtuality of the spacelike parton line would still force the complete cascade to reassemble. Since the virtuality of the cascade probed is carried

by one single parton, it is possible to equate this spacelike virtuality with the Q^2 of the cascade, that is to be used e.g. in the AP equations. Further, coherence effects [8,9] guarantee that the Q^2 values of the partons along the main chain are strictly ordered, with the largest Q^2 values closest to the hard scattering.

Instead of having a treelike structure, treating all legs democratically, the cascade is reduced to a single sequence of branchings a→bc, where the a and b are on the main chain of spacelike virtuality and the c are on mass shell and do not branch. (Later we will include the possibility that the c may have positive virtualities $m_c^2 > 0$, which leads to the appearance of timelike parton showers.) This truncation of the cascade is only possible when it is known which parton actually partakes in the hard scattering: of all the possible cascades that exist virtually in the incoming hadron, the hard scattering will select one. To obtain the correct Q^2 evolution of structure functions, e.g., it is essential that all branches of the cascade be treated democratically. In Monte Carlo simulation of spacelike parton showers this is a major problem. If indeed the evolution of the complete cascade is to be followed from some small Q_0^2 up to the Q^2 of the hard scattering, it is not possible to handle kinematics exactly, since the virtuality of the various partons can not be found until after the hard scattering has been selected. An alternative is to make a random choice at each branching a→bc which of b and c is spacelike, and carry along as compensating weight a factor of 2 for each branching. In this way kinematics can be handled better, but it leads to large fluctuations in the overall weight of events and consequently to efficiency problems in the Monte Carlo approach. We refer to models of the kinds above as "forward" evolution schemes, since they follow a cascade from the initiator at low Q^2 towards the scattering parton at high Q^2, naively in the forward time sense (closer and closer to the hard scattering).

In forward evolution the amount of parton shower evolution affects the cross section for a hard scattering but, until the hard scattering has been selected according to the proper differential cross section, the upper Q^2 limit of the shower evolution is not known - a "vicious circle" [10]. Our proposed way out of this problem is "backward" evolution, i.e. to start with the hard scattering and successively reconstruct the parton showers that preceded it.

A hard scattering subprocess of the basic 2→2 type in hadronic interactions is characterized by three kinematical variables, conventionally x_1, x_2 and $\hat{t}$. For the production of a single W or Z the last variable is superfluous, but may be

used to characterize the angle of the subsequent two-body decay. These variables are distributed according to the generic cross section

$$d\sigma = \sum_{ijk} f_i(x_1,Q^2)\, f_j(x_2,Q^2)\, \frac{d\hat{\sigma}^k_{ij}}{d\hat{t}}(\hat{s},Q^2)\, dx_1\, dx_2\, d\hat{t} \tag{4}$$

Here $d\hat{\sigma}^k_{ij}/d\hat{t}$ is the parton-parton hard interaction cross section for the k:th subprocess for incoming partons i and j. The Q^2 dependence enters $d\hat{\sigma}/d\hat{t}$ only through the appearance of an $\alpha_s^2(Q^2)$ factor for a normal parton-parton scattering, which is reduced to $\alpha_s(Q^2)$ e.g. for $qg \to q\gamma$ and absent e.g. for $q\bar{q} \to Z^0$. The appearance of Q^2-evolved structure functions, on the other hand, exactly corresponds to an inclusive summation over all initial state parton showers. With Q^2-dependent structure functions available, the hard scattering can thus be selected once and for all. It then remains to reconstruct the initial parton showers that resulted in the two incoming partons i and j at x_1 and x_2. This will be done one step at a time, starting at the hard scattering and retracing the evolution back to the shower initiators. Since the Q^2 of the hard scattering is known from the start in this case, the problems of the "vicious circle" above cease to exist. Further, the separation of spacelike and timelike partons is obvious in every step of the kinematical reconstruction, so neither approximate kinematics nor compensating weights are necessary.

2.2. Longitudinal Evolution

The AP equations express that, during a small increase dt there is a probability for a parton a with momentum fraction x' to become resolved into a parton b at $x = zx'$ and a parton c at $x'-x = (1-z)x'$. Correspondingly, during a decrease dt a parton b may be "unresolved" into a parton a. The relative probability dP_b for this to happen is given by df_b/f_b which, using eq. (1), becomes

$$dP_b = \frac{df_b(x,t)}{f_b(x,t)} = |dt|\, \frac{\alpha_s(t)}{2\pi} \sum_a \int \frac{dx'}{x'}\, \frac{f_a(x',t)}{f_b(x,t)}\, P_{a\to bc}\left(\frac{x}{x'}\right) \tag{5}$$

Summing up the cumulative effect of many small changes dt, the probability for no radiation exponentiates. Therefore one may define a form factor

$$\begin{aligned} S_b(x,t_{max},t) &= \exp\left\{ -\int_t^{t_{max}} dt'\, \frac{\alpha_s(t')}{2\pi} \sum_a \int \frac{dx'}{x'}\, \frac{f_a(x',t')}{f_b(x,t')}\, P_{a\to bc}\left(\frac{x}{x'}\right) \right\} \\ &= \exp\left\{ -\int_t^{t_{max}} dt'\, \frac{\alpha_s(t')}{2\pi} \sum_a \int dz\, P_{a\to bc}(z)\, \frac{x' f_a(x',t')}{x f_b(x,t')} \right\} \end{aligned} \tag{6}$$

giving the probability that a parton b remains at x from t_{max} to $t < t_{max}$.

It may be useful to compare this with the corresponding expression for forward evolution, either in a spacelike or a timelike shower. In the latter case $t = \ln(Q^2/\Lambda^2)$ has to be replaced by $t = \ln(m^2/\Lambda^2)$ or, for coherent showers, $t = \ln(E_a^2(1-\cos\theta_{bc})/\Lambda^2)$ [6]. For timelike evolution, the form factor

$$S_a(t_{max},t) = \exp\left\{ -\int_t^{t_{max}} dt'\, \frac{\alpha_s(t')}{2\pi} \sum_b \int dz\, P_{a\to bc}(z) \right\} \tag{7}$$

expresses the probability that a parton a does not branch between t_{max} and $t<t_{max}$. For forward spacelike evolution, i.e. t increasing, $S_a(t,t_{min})$ gives the probability that a does not branch between t_{min} and $t>t_{min}$. In the notation above, the ordinary Sudakov form factor is $S_a(t) = S_a(t,t_0)$ with t_0 a fixed lower cutoff.

The most obvious difference between S_b and S_a is the explicit appearance of structure functions in the former. This expresses the fact that the probability for a parton b to come from the branching of a parton a is proportional to the number of partons a present in the hadron, whereas the probability for a given parton a to branch, once present, is independent of this number. Thus the numerator $f_a(x',t')$ in S_b ensures that the parton composition of the hadron is properly reflected. As an example, when a gluon is chosen at the hard scattering and evolved backwards, this gluon is more likely to have been emitted by a u than by a d if the incoming hadron is a proton. Similarly, if a heavy flavour is chosen at the hard scattering, the denominator $f_b(x,t')$ will vanish at the Q^2 threshold of the heavy flavour production, which means that the z integral diverges and S_b itself vanishes, so that no heavy flavours remain below threshold.

In the compact notation above, an implicit difference of a factor two in some places is not readily visible. This factor comes since a branching removes one parton a but creates two partons b and c. More explicitly, when integrating $P_{g\to gg}(z)$ appearing in S_a, a factor 1/2 is to be included, since the two final gluons are identical, so that a branching with splitting variable z and one

with $1-z$ are equivalent. This is not so for S_b, where parton a in one case would be at $x'=x/z$ and in the other at $x'=x/(1-z)$. Correspondingly, whereas the $q\to qg$ ($g\to q\bar{q}$) kernel only appears in the quark (gluon) evolution for S_a, it appears both in the quark and gluon (antiquark) evolution for S_b.

A knowledge of S_b is enough to reconstruct the parton shower backwards. At each branching, three quantities have to be found: the t value of the branching (which also defines the virtuality Q^2 of parton b), the parton flavour a and the splitting variable z. This information may be extracted as follows.

(i) If parton b partook in the hard scattering at a scale t_{max} or branched into b'c' at this scale, the probability that b is still resolved at the lower cutoff scale t_0 is given by $S_b(x,t_{max},t_0)$ with $x=x_b$. If a branching $a\to bc$ does take place between t_{max} and t_0, the probability distribution in t is given by $dS_b(x,t_{max},t)/dt$. In Monte Carlo language, the t value may be found by solving the equation $S_b(x,t_{max},t) = R$, with R a random number evenly distributed between 0 and 1; the no branching case then corresponds to $R < S_b(x,t_{max},t_0)$.

(ii) For a given t of a branching, the relative probabilities for the different allowed branchings $a\to bc$ are given by the z integrals

$$\int dz\, P_{a\to bc}(z)\, \frac{x'f_a(x',t)}{xf_b(x,t)} \tag{8}$$

(iii) Finally, with t and a known, the probability distribution in the splitting variable $z = x/x' = x_b/x_a$ is given by the integrand above.

In practice, a numerical integration over x' and t' would be too time-consuming. A convenient Monte Carlo procedure is based on finding an analytically integrable fuction that is everywhere larger than the integrand in eq. (6). For the gluon and sea quark structure functions one may assume that $x'f_a(x',t')$ is a falling function of x' so that, since $x'>x$, $x'f_a(x',t')/(xf_b(x,t')) \leqslant f_a(x,t')/f_b(x,t')$. This does not hold for valence quarks, where one instead e.g. can use that $x'^{1/2}f_a(x',t')$ normally is falling with x', so that $x'f_a(x',t')/(xf_b(x,t')) \leqslant z^{-1/2}f_a(x,t')/f_b(x,t')$. In performing the z integral, it is also convenient to replace the numerators in $P_{a\to bc}(z)$ by their maximum values. If the t' dependence of the a and b structure functions is neglected, i.e. the ratio $f_a(x,t')/f_b(x,t')$ is evaluated at $t'=t_{max}$ (and then multiplied by some constant factor $\geqslant 1$ to provide a safety margin), the integration over t' only involves $\alpha_s(t')$ and may be performed analytically. This gives an approximate S_b, for which the equation $S_b(x,t_{max},t) = R$ may be solved analytically to yield a t. The

approximate z integrals can be used to select channel $a\to bc$ and the approximate form of $P_{a\to bc}(z)$ and the structure function ratio to select z; because of the approximations made the z integral is analytically invertible. The probability that this set of t, a and z values should be kept is given by the ratio of the correct to the approximate integrand in eq. (8). If the set is rejected, the upper limit t_{max} is to be put equal to the t value rejected, and the procedure iterated until a set is accepted or the t_0 cutoff scale is reached. For a heavy flavour b, the t' evolution can not be neglected in finding an upper limit to the ratio of structure functions close to threshold t_{thr}. One possible method is to evaluate the structure function ratio at t_{max} and at $(t_{max}+t_{thr})/2$ and use whichever is the larger to provide an upper bound on the integrand. If a t value above $(t_{max}+t_{thr})/2$ is selected, the probability for acceptance is evaluated as usual, but if the t value is smaller then $(t_{max}+t_{thr})/2$ is chosen as the new t_{max} value and the procedure is repeated. With a fictitious $t_{thr} < t_0$ this algorithm could also be used to control the t' evolution of nonheavy flavours, if need be.

A comment on soft gluon emission. Nominally the range of the z integral in S_b is $x \leqslant z \leqslant 1$. The lower limit corresponds to $x' = x/z = 1$, and does not cause any problems. At the upper cutoff $z = 1$ the AP kernels $P_{q\to qg}(z)$ and $P_{g\to gg}(z)$ diverge. This is the soft gluon singularity: the energy fraction carried by the emitted gluons vanish, $x_g = x'-x = (1-z)x' = (1-z)x/z \to 0$ for $z \to 1$. In order to calculate the integral over z in S_b, an upper cutoff $z_{max} = x/(x+\varepsilon)$ is introduced, i.e. only branchings with $z \leqslant z_{max}$ are included in S_b. Here ε is a small number, typically chosen so that the gluon energy $x_g s^{1/2}/2 \geqslant \varepsilon s^{1/2}/2 = 2$ GeV. The effects of partons with $z > z_{max}$ can be estimated as follows. In the limit $z \to 1$ the $q\to qg$ and $g\to gg$ kernels may be written as $P_{a\to ag}(z) = K_{a\to ag}/(1-z)$ with $K_{q\to qg} = 8/3$ and $K_{g\to gg} = 6$. The average relative parton energy removed by such soft gluon emission during a small change dt can be expressed as an effective $\langle z_{soft}\rangle$,

$$\begin{aligned}\langle z_{soft}\rangle &\approx 1 - dt\,\frac{\alpha_s(t)}{2\pi}\int_{x/(x+\varepsilon)}^{1} dz\, P_{a\to ag}(z)\,\frac{x'f_a(x',t)}{xf_a(x,t)}\,\frac{x'-x}{x} \approx \\ &\approx 1 - dt\,\frac{\alpha_s(t)}{2\pi}\,\frac{\varepsilon}{x+\varepsilon}\,K_{a\to ag}\end{aligned} \tag{9}$$

Between two hard branchings t_a and t_b, the average z value due to soft gluon emission is then

$$\langle z_{soft}(t_a,t_b)\rangle \approx \exp\left\{ -\int_{t_a}^{t_b} dt\, \frac{1}{b_0 t}\, \frac{\varepsilon}{x+\varepsilon}\, K_{a\to ag} \right\} = \left\{\frac{t_b}{t_a}\right\}^{\frac{K_{a\to ag}}{b_0}\frac{\varepsilon}{x+\varepsilon}} \tag{10}$$

with $b_0 = (33-2n_f)/6$, i.e. $\alpha_s(t) = 1/(b_0 t)$. When a branching $a\to bc$ is found, with a given z_{hard} defined by the ε-regularized S_b, the average effects of soft gluon emission can be included by defining $z = z_{hard}\cdot\langle z_{soft}(t_a,t_b)\rangle$ as the effective splitting variable. By varying the ε value, we have verified that the soft gluon effects indeed are small for reasonable ε values.

The procedure described in this section may be iterated to yield a sequence of branchings, stretching backwards from the hard scattering to the shower initiators at the low cutoff scale Q_0^2, which typically is taken to be 4 GeV^2 in structure function parametrizations. The parton virtualities Q^2 are arranged in falling order, with the actual virtuality t of one parton giving the upper limit t_{max} for the next in the chain, and with parton energy fractions x increasing at each step.

2.3. Transverse Evolution

We have above seen that two parton lines may be defined, stretching back from the hard scattering to the initial incoming hadron wavefunctions at small Q^2. Specifically, all parton flavours i, virtualities Q^2 and energy fractions x may be found. The exact kinematical interpretation of the x variable is not unique, however. For partons with small virtualities and transverse momenta, all definitions are essentially equivalent, but differences of order Q^2/s and p_T^2/s will appear for the partons close to the hard scattering.

One possibility is to use lightcone variables, i.e. interpret x as $E+p_z$ fraction for the parton shower developing along the +z direction and $E-p_z$ for the other one (with the two incoming hadrons aligned along the ±z axis). With such a choice the $\hat{s}$ of the hard scattering becomes

$$\hat{s} = x_1x_2s - Q_1^2 - Q_2^2 + \frac{Q_1^2Q_2^2}{x_1x_2\hat{s}} - (p_{x1}+p_{x2})^2 - (p_{y1}+p_{y2})^2 \tag{11}$$

The implications of the last two terms is that two partons which have built up large transverse momenta in essentially the same direction may combine to give a small $\hat{s}$, even when x_1x_2s is large. This is unfortunate for two reasons. First, since the Q^2 scale of the hard scattering is bounded by $\hat{s}$ (up to some

factor of order unity), it may well happen that Q_1^2 and/or Q_2^2 are larger than this scale, thus breaking our desire to have the Q^2 values strictly ordered (see also section 2.4). Second, from a practical point of view, the hard scattering cross section, which depends on $\hat{s}$, could not be calculated until the two incoming parton showers are completely known.

An alternative is the "$\hat{s}$ approach": to require that $\hat{s} = x_1x_2s$, both at the hard scattering and at any lower scale, i.e. $\hat{s}(Q^2) = x_1(Q^2)x_2(Q^2)s$, where $x_1(Q^2)$ and $x_2(Q^2)$ are the x values of the two resolved partons at the given Q^2 scale. In practice this means that, at a branching with the splitting variable z, the total $\hat{s}$ has to be increased by a factor 1/z in the backward evolution. As an example, referring to Fig. 2, the z value of the branching 3→1+4 is given by $z = (p_1+p_2)^2/(p_3+p_2)^2$. Further, branchings on the two spacelike main chains are to be interleaved into one single sequence in falling Q^2 order.

For the case of initial state photon radiation in e^+e^- annihilation, it has been shown [18] that the first order cross section factorizes into the correct AP splitting kernel $P_{e\to e\gamma}(z=\hat{s}/s)$ times the lowest-order cross section at the reduced energy $\hat{s}=zs$, independently of the detailed nature of the hard interaction. Also for the QCD case some simple toy models have been studied with similar results [13]. Because of these indications, and because of the problems with lightcone variables noted above, we have adopted the $\hat{s}$ approach.

For a reconstruction of the complete kinematics in this approach, one should start with the hard scattering, for which $\hat{s}$ has been chosen according to the hard scattering matrix element. By backward evolution, the virtualities Q_1^2 and Q_2^2 of the two interacting partons are reconstructed. Initially the two partons are considered in their CM frame, coming in along the ±z directions, Fig. 2. Then the four-momentum vectors p_1 and p_2 have the nonzero components

$$E_{1,2} = \frac{\hat{s} \pm (Q_2^2-Q_1^2)}{2\,\hat{s}^{1/2}}$$
$$p_{z1} = -p_{z2} = \left\{\frac{(\hat{s}+Q_1^2+Q_2^2)^2 - 4Q_1^2Q_2^2}{4\hat{s}}\right\}^{1/2} \tag{12}$$

with $(p_1+p_2)^2 = \hat{s}$.

If, say, $Q_1^2 > Q_2^2$, then the branching 3→1+4 is the one that took place "closest" to the hard scattering, and the one to be reconstructed first. With the four-momentum p_3 known, $p_4 = p_3-p_1$ is automatically given, so there are

four degrees of freedom. One corresponds to a trivial azimuthal angle around the z axis. The z splitting variable for the 3→1+4 vertex is found at the same time as Q_1^2, and provides the constraint $(p_3+p_2)^2 = \hat{s}/z$. The virtuality Q_3^2 is again given by backward evolution.

One degree of freedom remains to be specified, and this is related to the possibility that parton 4 initiates a timelike parton shower, i.e. may have a nonzero mass. The maximum allowed mass-squared $(m_4^2)_{max}$ is found for a collinear branching 3→1+4. In terms of the combinations

$$\begin{aligned} s_1 &= \hat{s} + Q_2^2 + Q_1^2 \\ s_3 &= \frac{\hat{s}}{z} + Q_2^2 + Q_3^2 \\ r_1 &= \{s_1^2 - 4Q_2^2Q_1^2\}^{1/2} \\ r_3 &= \{s_3^2 - 4Q_2^2Q_3^2\}^{1/2} \end{aligned} \tag{13}$$

one obtains

$$(m_4^2)_{max} = \frac{s_1s_3-r_1r_3}{2Q_2^2} - Q_1^2 - Q_3^2 \tag{14}$$

which, for the special case of $Q_2^2=0$, reduces to

$$(m_4^2)_{max} = \{\frac{Q_1^2}{z} - Q_3^2\} \{\frac{\hat{s}}{\hat{s}+Q_1^2} - \frac{\hat{s}}{\hat{s}/z+Q_3^2}\} \tag{15}$$

With the maximum virtuality given, standard timelike parton shower algorithms may be used to give the development of the subsequent cascade, including the actual mass m_4^2, with $0 \leq m_4^2 \leq (m_4^2)_{max}$.

Using the further relation $m_4^2 = p_4^2 = (p_3-p_1)^2$, the momentum of parton 3 (in the CM frame of partons 1 and 2) may now be found as

$$\begin{aligned} E_3 &= \frac{1}{2\hat{s}^{1/2}} \{\frac{\hat{s}}{z} + Q_2^2 - Q_1^2 - m_4^2\} \\ p_{z3} &= \frac{1}{2p_{z1}} \{s_3 - 2E_2E_3\} \\ p_{T3}^2 &= E_3^2-p_{z3}^2+Q_3^2 = \{(m_4^2)_{max} - m_4^2\} \frac{\frac{1}{2}(s_1s_3+r_1r_3) - Q_2^2(Q_1^2+Q_3^2+m_4^2)}{r_1^2} \end{aligned} \tag{16}$$

(For p_T^2 the expression $E_3^2-p_{z3}^2$ often involves the subtraction of two almost equally large numbers, so the last expression is essential for numeric stability in Monte Carlo applications.)

The requirement that $m_4^2 \geq 0$ (or $\geq m_q^2$ for heavy flavours) imposes a constraint on allowed z values. This constraint can not be included in the choice of Q_1^2, where it logically belongs, since it also depends on Q_2^2 and Q_3^2, which are unknown at that point. It is fairly rare (in the order of 10% of all events) that an unallowed z value is generated, and when it happens it is almost always for the two branchings closest to the hard interaction: for $Q_2^2=0$ eq. (15) may be solved to yield $z \leq \hat{s}/(\hat{s}+Q_1^2-Q_3^2)$, which is a more severe cut for $\hat{s}$ small and Q_1^2 large. Therefore an essentially bias-free way of coping is to redo completely any initial state cascade for which this problem appears.

This completes the reconstruction of the 3→1+4 vertex. The 3-2 subsystem may now be boosted to its rest frame and rotated to bring 3 and 2 along the ±z direction. When the next vertex is considered, 5→2+6 or 7→3+8 in Fig. 2, the 3-2 system will fill the function the 1-2 system did above, and the 3→1+4 branching does not enter. After a number of steps, the two outermost partons have virtualities $Q^2 < Q_0^2$, and one may e.g. put these $Q^2 = 0$. Up to small corrections from primordial k_T, a final boost will bring the partons from their CM frame to the overall CM frame, where the x values of the outermost partons agree also with the lightcone definition.

2.4. Further Aspects

In the sections above, Q^2 has been used to denote a parton virtuality or an argument in α_s and structure functions, in spacelike showers, the hard scattering and timelike showers (with $Q^2 \to m^2$ for the virtuality in the latter case). It is in the nature of the perturbative description of QCD that the definition of Q^2, e.g. in α_s, is not unique. Rather, any choice is allowed in lowest order, and will be compensated by higher order corrections; a successful choice of Q^2 scale is one for which these corrections are small. Within the framework of our approach, where the initial and final state radiation is considered separately from the hard interaction, a fully consistent choice may not be possible. We have therefore allowed for a number of slightly different interpretations of the kinematical variables.

In particular, loop calculations tend to indicate that the proper argument for α_s is not Q^2 but $k_T^2 = (1-z)Q^2$ [9]. For a branching a→bc with a and c massless and $Q^2 = -m_b^2$, k_T has the interpretation of the transverse momentum of the branching if z is chosen as lightcone fraction. (In timelike showers, the suggested choice as α_s argument is $k_T^2 = z(1-z)Q^2$, where again k_T has an interpretation as transverse momentum, now for $m_b = m_c = 0$.) The most straightforward way to take into account this uncertainty in the Q^2 scale is to evaluate α_s (and structure functions) at a fixed fraction of Q^2; indeed, our default procedure has been to use $Q^2/4$, remembering that z values close to 1 are more likely. For comparison, α_s may be evaluated at k_T^2, in which case the lower cutoff of the shower also has to be implemented on k_T^2 to avoid unphysical α_s values.

Indeed, the complete parton shower evolution may be interpreted in terms of k_T^2, i.e. one may have $t = \ln(k_T^2/\Lambda^2)$ in eqs. (1) - (10), and only convert to $Q^2 = k_T^2/(1-z)$ for the kinematics reconstruction. In particular, this implies that branchings are ordered in k_T^2 rather than Q^2. Studies in some specific regions of phase space indicates that this might be a better choice [19]; although the situation is far from clear. It should also be remembered that the choice of the various k_T^2 values do not decouple completely: again using the lightcone z choice with $m_c = 0$, a constraint $Q_a^2 \leqslant Q_b^2/z$ is obtained. In the terminology of section 2.3, the exact form of this constraint becomes

$$Q_3^2 \leqslant \frac{1}{2}\left(\frac{1}{z}+1\right) Q_1^2 + \frac{1}{2}\left(\frac{1}{z}-1\right) \left\{Q_2^2 - \hat{s} + \left(s_1^2 + 8Q_1^2Q_2^2 \frac{z}{1-z}\right)^{1/2}\right\} \tag{17}$$

which has to be checked in the generation of k_{T3}^2. This requirement is uninteresting when Q^2 is assumed to be the evolution variable, since the strict ordering of Q^2 values required by coherence effects [8,9] is a stronger constraint by itself.

For W and Z production, customarily m^2 is taken to set the scale of the hard interaction, while for hard QCD interactions alternatives like $-\hat{t}$, $2\hat{s}\hat{t}\hat{u}/(\hat{s}^2+\hat{t}^2+\hat{u}^2)$ or $\hat{p}_T^2 = \hat{t}\hat{u}/\hat{s}$ have been suggested. The latter three all coincide for small scattering angles, and we will mostly use $\hat{p}_T^2$. There is then a discrepancy of a factor 4 for production at 90° between the W and the QCD cases: $m^2 = \hat{s} = 4\hat{p}_T^2$. This would certainly be allowed, since W production is entirely in the s channel, whereas QCD interactions also receive t and u channel contributions. In order to obtain a smooth joining to the parton shower conventions, the actual choice here has been to use $m^2/4$ and $\hat{p}_T^2$, respectively, as α_s and structure function scale for the hard interaction, but let m^2 and $4\hat{p}_T^2$ set the scale for maximum virtualities allowed in the timelike

and spacelike parton showers.
In our algorithms, the initial and final state showers are constructed to have smaller virtualities than the hard scattering. The reasoning behind this is as follows (Fig. 3). Consider a hard scattering 1+2→1'+2' via the interchange of a parton 0, e.g. in the t channel. Here parton 1 may be off mass-shell, due to an initial state branching 3→1+4. Alternatively one could call the subprocess 3+0→4+1' the hard scattering, with 1 as propagator and 2→2'+0 as an initial state branching. In principle, either description is allowed, but the probability for a given final state must not be double-counted. The requirement that the hard scattering is the subprocess with the largest Q^2 value defines an ordering so that this problem may be avoided.

This comment applies not only to QCD processes, but also to W or Z production, as follows. The most reliable description of W production at large transverse momenta is provided by the matrix elements for the 2→2 processes q+g→q'+W and $q+\bar{q}'\to g+W$ [20]. The process q+g→q'+W may be time ordered either as an initial state radiation $g\to q'+\bar{q}'$ followed by a hard interaction $q+\bar{q}'\to W$ or as an initial state radiation q→q'+W followed by q'+g→q' or as an s-channel graph q+g→q→q'+W, and correspondingly for $q+\bar{q}'\to g+W$. Additionally, interference terms between different time orderings are present. For small transverse momenta, initial state radiation of an on-mass-shell W is suppressed by propagator effects and our simple picture is recovered, with the W always produced at the hard interaction. This is no longer true for p_{TW} comparable to m_W, where our neglect of the initial state radiation of W bosons should lead to an underestimation of the correct cross section.

The argument above is not the only reason why one might expect our approach to work less well for large p_{TW}. Further assumptions include the use of process-independent Altarelli-Parisi splitting kernels and a specific choice for the interpretation of the z splitting variable. Any errors in these assumptions must vanish in the collinear limit, but might be large for $p_{TW} \geqslant m_W/2$.

Whereas coherence effects along the main chain of spacelike partons are well understood, the same can not be said on the subject of "associated timelike showers", i.e. those side branchings to the main chain that initiate timelike showers (the word "associated" is used to distinguish them from the ordinary timelike showers initiated by the two partons emerging from the hard scattering). Above we derived formulae for $(m_4^2)_{max}$, which give the kinematical upper limit for such showers. It is not known to what extent this full phase space is available for shower development. Does e.g. angular ordering

requirements enter not only in the development of each timelike shower separately, but also in the correlation between the different showers, thus decreasing the total amount of shower development? In the following we will often compare differences, which never will be that large, between having no timelike showers at all or having showers as allowed by the full phase space, thus covering the two extremes.

Because of confinement effects, the parton production we have been describing so far is not directly observable. Rather, the hadrons observed come from the fragmentation of partons produced in initial and final state showers, as well as "spectator" beam jets. Our scheme for the fragmentation of these is the Lund string model [21], which is well established in the fields of e^+e^- annihilation and leptoproduction. However, the uncertainties are far larger in the field of hadronic collisions. One question that has to be answered is that of colour flow: how are the partons that emerge from a hard scattering connected with strings? This subject has been extensively studied in [22], and we do not repeat the discussion here. In the leading log description of parton showers, where only simple branchings $a \to bc$ are included, the rules for the colour flow are well defined, but corrections could come from higher orders. Another major uncertainty is the structure of the low-p_T background to the hard interactions. In [23] we argued that there is a sizeable probability for several parton-parton interactions in one single hadron-hadron collision, and that the probability for additional interactions is particularly large for events which contain a very hard interaction. We will, at some points, use this model to show how large uncertainties are caused by extra "soft" particle production.

Finally, a note on the Monte Carlo. The program used to simulate the hadron physics aspects, including hard interactions and spacelike showers is found in PYTHIA version 4.3 [22,24], whereas timelike showers and fragmentation are handled with JETSET version 6.2 [7]. Both programs are available to interested parties.

3. W and Z Production

As mentioned in the introduction, W and Z production provides a convenient testing ground for initial state radiation calculations. In section 3.1 we present comparisons between our model and existing UA1 and UA2 data, and in 3.2 we compare with other theoretical calculations. Finally, 3.3 contains some

further studies within the framework of our model, with suggestions for other distributions that could be studied.

3.1. Comparisons with Data

Results on W and Z production have been presented by the UA1 [1] and the UA2 [2] collaborations. These data have been collected, roughly 1/3 at a CM energy $s^{1/2}$ = 546 GeV and 2/3 at 630 GeV, so we have chosen to compare with events generated at an energy of 600 GeV. A major advantage of the backwards evolution scheme is that the W mass may be chosen according to the basic Breit-Wigner shape, somewhat modified by structure function effects. The nominal W mass 83 GeV and total width 2.8 GeV have been used throughout.

In Fig. 4 a comparison is presented between UA1 data, UA2 data and model calculations for the normalized p_T spectrum of $W \to e\nu_e$ events, $(1/N)dN/dp_{TW}$. It would seem that the model curve (dashed) is too narrow, i.e. the probability for low p_{TW} is overestimated. The experimental distribution is significantly smeared, however: the neutrino is not directly observable, so the W transverse momentum is reconstructed from the hadrons by momentum conservation, $\bar{p}_{TW} = -(\Sigma\bar{p}_T)_{hadrons}$, with associated calorimetric fluctuations and with some particles being missed altogether. In order to estimate these effects, an attempt has been made to reproduce some of the UA1 conditions, to provide a smeared version of our curves. No similar study has been performed for UA2, but we expect smearing effects to be of comparable magnitude for the two detectors.

The following detector corrections and event reconstruction criteria have been applied.

(i) Particles within 0.2° of the beam axis are removed. The transverse momentum of remaining particles, except the electron, is summed up to give $-\bar{p}_{TW}$.

(ii) Smearings ΔE_x and ΔE_y are chosen according to independent Gaussian distributions, each with width $0.4 \cdot (\Sigma E_T)^{1/2}$, where ΣE_T is the sum of transverse momenta for all detectable particles, again except the electron.

(iii) An event is retained only if the following event selection criteria, intended to remove fake electron candidates or electrons from bottom and charm decays in QCD jets, are fulfilled:

(a) both the electron and the missing transverse energy must exceed 15 GeV;

(b) the electron must be at least 5° away from the beam axis;

(c) the summed transverse momentum of all particles within $\Delta R = ((\Delta\eta)^2+(\Delta\phi)^2)^{1/2} < 0.4$ of the electron must be less than 10% of the electron transverse energy ("loose isolation");

(d) the summed transverse momentum within $\Delta R < 0.7$ of the electron must not exceed 3.2 GeV ("tight isolation").

The result after these corrections is shown as the full curve in Fig. 4. The region of small p_{TW} is depleted by smearing effects, so that agreement with data is improved significantly. The region of large p_{TW}, and hence above-average jet activity, is somewhat suppressed by the electron identification cuts, (iii) above, so that the overall shift of $\langle p_{TW}\rangle$ is not large.

A compilation of $\langle p_{TW}\rangle$ values is presented in Table 1, to show how (in)sensitive results are to the various assumptions made. The mean p_{TW} in the model ("raw") is complemented with the smeared result (after (i) and (ii) above) and the result after event selection criteria ((iii) above) have also been applied.

The standard results, corresponding to Fig. 4, are shown in line 1. These are based on using the EHLQ1 structure functions with $\Lambda = 0.2$ GeV, whereas lines 2 and 3 are for EHLQ2 with $\Lambda = 0.29$ GeV and DO2 with $\Lambda = 0.4$ GeV, respectively. As expected, $\langle p_{TW}\rangle$ increases with increasing Λ value.

Whereas the standard results are based on allowing conventional timelike showers to develop on the timelike side branches of the spacelike main chain, in line 4 a coherent branching scheme is used instead, with no timelike showers at all in line 5. As is readily visible from eq. (16), a smaller m^2 leads to a larger p_T^2, so the increase in $\langle p_{TW}\rangle$ is to be expected when no timelike showers are allowed. The maximum virtuality that should be used in a coherent branching scheme is not as unambiguously defined as for the conventional case; it is possible that part of the discrepancy between the two shower schemes is due to such problems rather than any large inherent difference. The effects due to our resummation of soft gluon emission (eq. (10)) are minor, as seen by the results in line 6, where such effects are not included.

In lines 7 and 8 the α_s argument is changed from the standard choice $Q^2/4$ to Q^2 and $k_T^2 = (1-z)Q^2$, respectively. The trend towards somewhat larger $\langle p_{TW}\rangle$ for smaller α_s argument is clear. It seems that the argument $Q^2/4$ on the average is somewhat smaller than k_T^2. On the one hand, the $1/(1-z)$ singularity in the

splitting functions favours z close to 1 and hence $k_T^2 \ll Q^2$, on the other the main contribution to p_{TW} comes from branchings with large k_T, i.e. z not too close to 1, i.e. $k_T^2 \approx Q^2$, with $k_T^2 \approx Q^2/4$ a reasonable compromise. The possibility of performing the evolution entirely in terms of k_T^2, rather than in Q^2, is explored in lines 9 and 10. The difference is that in the latter case the Q^2 values at the branchings closest to the hard interaction are required to be smaller than m_W^2 (as is standard for evolution in Q^2), whereas in the former case only the k_T^2 are thus constrained; a small difference, as it turns out. The results are particularly close to those obtained using $\alpha_s(k_T^2)$, showing that the main effect is in the choice of α_s argument rather than in replacing dQ^2/Q^2 by dk_T^2/k_T^2.

Surprisingly, the strict ordering of Q^2 virtualities in the spacelike cascade, which is due to coherence effects rather than kinematical constraints, is fairly unimportant for $\langle p_{TW}\rangle$. This is shown by line 11, where virtualities are not required to be ordered, but rather t_{max} in eq. (6) is given by the largest kinematically allowed value, cf. eq. (17); the maximum virtuality of the two partons at the hard interaction is still assumed to be given by the hard interaction Q^2 value, however. The reason for the small difference is that the nonordered Q^2 evolution leads to more branchings, but the p_T in each branching is less. While the $\langle p_{TW}\rangle$ is essentially unchanged, the low end part of the p_{TW} spectrum is depleted for nonordered evolution, since the probability of not having any branching at all is decreased.

The sensitivity of $\langle p_{TW}\rangle$ to the choice of starting virtuality Q^2_{max} and shower cutoff virtuality Q^2_{min} is demonstrated in lines 12-15; the standard values are $Q^2_{max} = m_W^2$ and $Q^2_{min} = 4$ GeV^2. The standard inclusion of primordial k_T for the shower-initiating partons, using a Gaussian distribution in x and y separately so that $\langle p_T^2\rangle = 2\cdot(0.44\text{ GeV})^2$, does not affect $\langle p_{TW}\rangle$, line 16, but in a dN/dp_{TW} plot it leads to an unappealing δ peak at $p_{TW} = 0$ from those events where no radiation at all took place above Q^2_{min}.

Finally, the question of multiple interactions, i.e. parton-parton interactions in addition to the one that produced the W, does not directly affect the W production properties, but only how dirty the "beam jet" background is, and hence how much experimental smearing may be expected. Since the expectation is that W production events are more central (i.e. have smaller impact parameters) than average minimum bias events, we have used the model of [23] with a factor two higher multiple interaction probability as default. Lines 17 and 18 shows the consequences of varying this between

nothing at all and a factor four enhancement.
We conclude that the result shown in Fig. 4 are not crucially dependent on any of the assumptions made in the model. Although not shown, this turns out to be true for the p_{TW} distributions themselves as well, and not just the mean values. Considering the large statistical and systematic errors in the experimental data, it would therefore be difficult to distinguish between the different variations.

In order to find the jets associated with W production, again an algorithm closely modelled on that of UA1 was used:
(i) A detector, assumed to stretch between pseudorapidities $-3 < \eta < 3$ is divided into a number of cells, 50 in pseudorapidity and 24 in azimuth.
(ii) The energy deposited in each cell is summed up. A detector cell resolution behaving like $0.8 \cdot E_T^{1/2}$ is assumed; therefore a smearing ΔE_T is chosen according to a Gaussian with width as above. The tails are cut off so that the energy is never negative or larger than twice the true energy.
(iii) The cell with the largest E_T is found. All cells within $\Delta R < 1$ and with $E_T > 2.5$ GeV are combined, to find the E_T-weighted center, which defines the cluster axis.
(iv) The E_T of all further cells within $\Delta R < 1$ of the cluster axis are added to define a cluster energy. If the E_T exceeds 5 GeV and the axis has $|\eta| < 2.5$, a jet is defined.
(v) Cells assigned to a jet are removed from further consideration. The steps (iii) and (iv) are repeated for the unassigned cell with largest E_T, until all cells with $E_T > 2.5$ GeV have been tried as jet initiators.

The fraction of events that contain jets is shown as a function of p_{TW} in Fig. 5. Again our detector-smeared curve should primarily be compared with the UA1 results. Smearing effects tend to raise the number of jets reconstructed: since the spectrum $d\sigma/dp_{Tjet}$ is falling with p_{Tjet}, a symmetric smearing will lead to more clusters migrating up past 5 GeV than down past it.

In Table 1 the fraction of events with 1, 2; 3 and 4 jets, as well as the mean transverse momentum of these jets, is compared for UA1 data and the different model variations. The conclusion is that the results are not overly sensitive to the details of the model, but fairly sensitive to the effects of detector smearing (and how this smearing is implemented in detail, e.g. with respect to the high-end tail of energy fluctuations), especially for the rate of multijet events (compare the two lines of case number 1 with and without smearing). Until corrected experimental data are presented, and until the statistical

significance is improved, no firm conclusions can therefore be drawn.
A further check is provided by the distribution in polar angle of the jets in W events. More precisely, a θ^* angle has been defined between the jet and the average beam direction in the rest frame of the W and the jet(s). Again, detector smearing and jet reconstruction à la UA1 has been used, including a reconstruction of the neutrino longitudinal momentum based on requiring the W mass for the νe system, with the lower Feynman x value chosen in cases of ambiguity. The result of this comparison is presented in Fig. 6, and good agreement is observed.

From the comparisons above we conclude that our model is able to provide a very good description of present experimental data on W production, given the limited statistics available so far.

3.2. Comparisons with other Calculations

Since a number of papers have been published on the subject of W production, it may be useful to compare with some of the results obtained in these, to point out the broad agreement obtained, but also the presence of some discrepancies. A complete coverage of existing calculations has not been strived for.

A simple factorized form for the n-gluon emission probability is used by Halzen, Martin, Scott and Tuite in [25], to give an exponentiated form for the total p_T of the Z^0, and also a form for the summed transverse energy of recoiling radiated partons. The results are shown in Fig. 7, where Owens-Reya structure functions with $\Lambda = 0.5$ GeV [26] have been used. For comparison, we present results based on GHR structure functions (the difference is not expected to be large, cf. our studies above), without the inclusion of associated timelike parton showers, which are not included in these analytical calculations. The shape of the Z p_T spectrum agrees fairly well, except for some small differences above 30 GeV (cf. our discussion in section 2.4), whereas the total E_T of associated partons seems to be roughly 2 GeV smaller in our model than in the calculation of Halzen et al. The reason for this discrepancy is not known, but could be related to the resummation of very soft gluon emission, a region that is not included in Monte Carlo calculations.

A series of detailed studies have been presented by Altarelli, Ellis, Greco and Martinelli [27]. Here the results of higher order loop calculations have been included to yield predictions, not only for the p_{TW} shape, but also for the absolute normalization, the "K factor". These factors can not be predicted within our Monte Carlo approach, so in Fig. 8 we have compared normalized distributions $(1/\sigma)d\sigma/dp_{TW}$. Results at 630 GeV agree fairly well, whereas the Monte Carlo curves are above the analytic calculations at 1.6 and 10 TeV (and even more so at 20 TeV, not shown) for $p_{TW} < 50$ GeV, an effect which is compensated by a more sizeable tail to large p_T in the analytic formulae. This does point to the fact that the Monte Carlo methods are not entirely reliable for transverse momenta in the order of the mass of the produced object, as discussed above. The peaks of the $d\sigma/dp_{TW}$ distributions are systematically displaced, so that the analytic peaks are typically sitting 1 GeV higher than the Monte Carlo ones.

A calculation in the same spirit, but with somewhat different assumptions as to details, is presented by Davies, Webber and Stirling [28]. Since their results are normalized to a given experimental luminosity, we have arbitrarily introduced an effective "K factor" of 2 to bring the overall normalization into better agreement. The results of this comparison are shown in Fig. 9, using two different structure function sets. Some discrepancies are readily visible. The analytic results are much more strongly peaked in the $p_{TW} = 1 - 4$ GeV region than are the Monte Carlo curves, whereas the position of the peak agrees fairly well. This implies that the Altarelli et al. and the Davies et al. analytic calculations do tend to give small but significant differences, with our results somewhere in between (in terms of where the bulk of the cross section is located). Further, the analytic results of Davies et al. indicate a very large dependence on the choice of structure functions (and Λ value), whereas differences are far smaller in the Monte Carlo results. In the latter, the effects of the associated timelike showers tend to partially counteract the naive Λ dependence: a larger Λ gives a more extensive shower development, which works to reduce p_{TW}. We do not see how one should explain the full discrepancy, however.

Three other Monte Carlo studies of W production have been presented. Of these, the one by Odorico [29] does differ in several of the basic assumptions, in particular the kinematics is implemented fairly differently, in terms of lightcone variables and without explicit four-momentum conservation at each branching. In addition, the coherence constraint of strict ordering in Q^2 is not included, but we have shown above that this does not seem to matter much

by itself. The results generally agree with ours, although it seems that Odorico obtains a slightly larger $\langle p_{TW}\rangle$. The second study is by Barger, Gottschalk, Ohnemus and Phillips [30], using the program of Gottschalk [13], which has large similarities with our program and tend to give similar results; however, fragmentation effects have not been included in this study. Finally, Paige and Protopopescu have included our basic algorithm of section 2.2 above, with slightly different kinematics, in the ISAJET program [31]. Since they use a fairly large cutoff, $Q^2_{min} = 36$ GeV^2, they have to introduce a Q^2-dependent "primordial k_T" which, for W/Z, is of the order of 3 GeV.

In summary, Monte Carlo and analytic calculations give good overall agreement. When details are studied, discrepancies do appear, not only between the Monte Carlo and the analytic results, but also e.g. between the analytic calculations themselves.

3.3. Further Studies

For practical applications, $d\sigma/dp_{TW}$ plots are very convenient, but the vanishing of the phase space for $p_T \to 0$ tends to dominate the shape of $d\sigma/dp_{TW}$. Therefore results for the phase space corrected distribution $(1/\sigma)d\sigma/dp^2_{TW}$ are presented in Fig. 10, as a function of p_{TW}. For this study, no intrinsic k_T effects have been included, but rather the cutoff scale Q^2_0 of parton showers has been decreased from 4 GeV^2 to 1 GeV^2, so that almost all events contain at least one branching. Most notable is the large difference in behaviour between inclusive (all rapidities) and central ($|y| \leq 0.5$) production of W, where the cross section at small p_{TW} falls far faster with CM energy in the latter case. The difference may be understood as follows. If a W is produced from a $q\bar{q}$ pair with a very asymmetric energy sharing, the faster of them will have a large x value. The rapid fall of structure functions for $x \to 1$ will tend to suppress initial state radiation on this side, and hence increase the probability to obtain a small p_{TW}.

The structure of the hadronic system accompanying a W has still not been studied in depth. Here we suggest two different distributions that could shed some light on this. The hadrons carry a total recoil of $-\bar{p}_{TW}$. A boost $\bar{\beta} = \bar{p}_{TW}/(s^{1/2}-E_W)$ will bring the hadrons to their transverse rest frame. In this frame one may study e.g. $dN/d\phi^*$, the particle distribution as a function of the azimuthal angle ϕ^* with respect to the W direction. In Fig. 11 this distribution is shown for some p_{TW} bins. The two spikes at π and 0 may have

been expected on general grounds, the first from jets recoiling against the W and the second due to the boost. The form of these spikes, as well as the fact that the population of the region around $\pi/2$ is independent of p_{TW}, is nontrivial.

The distribution of $<-\bar{p}_{TW}\bar{p}_{Thad}>/<p_{TW}^2>$ may be considered as a function of the azimuthal angle ϕ between the W and the hadrons in the event. Integrated over all angles, the result is unity. Events with smaller p_{TW} automatically give a lesser contribution to the total result. The distribution may be folded at $\phi = \pi/2$, i.e. W-hadron opening angles $\phi>\pi/2$ are included at $\pi-\phi$; this way all beam jet background sources that are not directly related to the W production, and are hence isotropic in ϕ, get subtracted. It also lessens the dependence e.g. on the choice of structure functions. The resulting distributions are shown in Fig. 12, with and without the inclusion of associated timelike showers. As expected, the latter case gives a narrower distribution, i.e. the $\bar{p}_T$ compensation is more strongly concentrated opposite to the W.

4. Jet Production

When moving away from the field of W/Z production, it becomes less straightforward to separate initial state radiation effects from effects of the hard interaction and of final state radiation.

One example is provided by the jet cross section, which we have studied using a simple cluster algorithm as described above, but without including energy smearing, since the published jet cross section [32] has been corrected for such effects. The naive jet cross section obtained without initial or final state radiation is increased by roughly a factor of 2.5 when initial state radiation effects are included, Fig. 13. Put another way, the transverse energy within the typical jet cone is increased by roughly 5 GeV. This is just an average figure, however. In an event without initial state radiation, the two high-p_T jets have opposite and balancing transverse momenta. Initial state radiation effectively induces a transverse boost, such that the transverse energy of one jet is reduced as that of the other is increased. Since the jet cross section falls rapidly with increasing E_T, the net effect is an increase in the jet cross section. Of course, there is also a probability that initial state radiation partons will overlap with one of the hard scattering partons.

The translation from the no-radiation to the radiation case does not just involve a simple transverse boost of the two hard scattering partons, however. Rather, each step of the initial state cascades is associated with one boost and one rotation of its own, the total effect of which may be decomposed into a rotation in the rest frame of the hard interaction, followed by an overall boost. Since the hard scattering matrix elements (specifically $qq\to qq$, $qg\to qg$ and $gg\to gg$) by themselves favour small scattering angles, those events where the rotation happens to increase rather than decrease the angle of the outgoing partons become proportionately more important. Of the factor 2.5 difference attributed to initial state radiation effects in Fig. 13, roughly half comes from the effective rotation and half from the effective boost. The relative importance of the two effects does vary with $x_T = 2E_T/s^{1/2}$, however, and at large x_T rotation effects are less important. Conversely, the effects of the boost tend to cancel in two-jet cross sections.

The inclusion of final state radiation tends in the opposite direction to that of initial state radiation: the energy of individual jets is decreased as a given initial parton may branch into several jets. For the chosen jet cone $\Delta R = 1$, jet cross sections are reduced by roughly a factor 1.5. With smaller jet cones, the reduction is larger, so that it is possible to choose jet cones for which initial and final state radiation effects cancel. The good agreement obtained between our final jet cross section and the UA1 results [32] is partly coincidental: it rests on assuming a K-factor of 1 and on neglecting various shifts included by UA1 to correct for stray particles migrating into or out of the experimental jet cone.

In the spirit of UA1 [33] a jet profile is defined by requiring a given minimum E_T within a jet cone $\Delta R = 1$ (with $|\eta_{jet}| < 2.5$), and then studying the transverse energy flow on the same side in azimuth ($|\phi-\phi_{jet}| < \pi/2$) as a function of pseudorapidity difference $\eta-\eta_{jet}$. It is illuminating to study the E_{Tmin} dependence of the jet profile. In [12,23] we showed that, for $E_{Tmin} = 35$ Gev, the transverse energy flow obtained by initial state radiation is too little to explain the "pedestal effect", and that an increased multiple parton-parton interaction probability has to be assumed for jet events. Since the main interest here is in the initial state radiation aspect, no multiple interaction effects have been included below, which means that the pedestal consistently will be too low, by an essentially E_{Tmin}-independent amount.

The interesting observation, Fig. 14a, is that the wings of the distribution, for $|\eta-\eta_{jet}| > 1$, are fairly E_{Tmin}-insensitive in the range $15 < E_{Tmin} < 90$ GeV, even with some indication that the wings are lowest for the highest E_{Tmin} values. Naively, one would have expected harder central interactions to be associated with more initial state radiation and hence produce higher wings. A number of effects combine to give the counterintuitive result of Fig. 14a.

In particular, there is a continuous change in the composition of interacting partons, from qq : qg : gg = 7% : 30% : 63% for E_{Tmin} = 15 GeV to 50% : 40% : 10% for E_{Tmin} = 90 GeV. In the Lund string framework, the removal of a quark from an incoming hadron leaves a remnant colour (anti)triplet, which is connected to the rest of the system by one string, whereas the removal of a gluon leaves a remnant colour octet that will be connected by two strings. Therefore the height of the rapidity plateau should be a factor two higher in the latter case, at least for not too large rapidities. If no initial or final state radiation is included, Fig. 14b, this effect dominates the picture, and leads to monotonically decreasing wings for increasing E_{Tmin}. A second result of the change in the parton composition is also that the amount of radiation is decreased with increasing E_T: the effective colour charge of the gluon is 9/4 larger than that of the quark, with a corresponding difference in the amount of initial state radiation.

Another aspect is that larger E_{Tmin} correspond to larger x values for the colliding partons; thus $x \geqslant 1/3$ for E_{Tmin} = 90 GeV at $s^{1/2}$ = 540 GeV. This reduces the range of the z integral in eq. (6), and hence the probability of a branching. In particular, the fact that the structure functions are rapidly falling for $x \to 1$ reduces the probability of obtaining a z value much lower than 1. Emission with $z \approx 1$ is not inhibited, but here the radiated partons have a small longitudinal and transverse momentum, the latter approximately given by $k_T^2 = (1-z)Q^2$, and do not contribute significantly to the E_T flow. The converse of the argument above is that an increase in the CM energy of the hadron collision will also increase the phase space available for hard initial state radiation. Therefore an increase in the wings of the jet profile is to be expected even if the E_{Tmin} scale, and hence the Q^2 scale, is kept fixed. This is illustrated in Fig. 15. The change with energy is somewhat amplified by, but not dominated by, the change in parton composition.

In closing this section, it is worth remembering that the smooth jet profiles displayed here constitute averages over many events, with the individual event often displaying a multijet structure. The details of this structure have yet

to be explored.

5. Conclusions

We have presented and discussed a model for initial state radiation, based on an iterative algorithm for successive parton branchings, which are considered in falling sequence of virtuality Q^2. There are two main virtues with this approach, as compared to more conventional analytical techniques. The first is that, in the leading log approximations we use, the initial state evolution does not depend on the nature of the hard interaction. Therefore, our algorithm can not only be used for present-day processes like W or jet production, but also for W/Z pairs, Higgs production, horizontal gauge bosons [34] etc. The second advantage is that our Monte Carlo approach allows the detailed study of events where many partons have been radiated, as well as straightforward inclusion of fragmentation effects.

W production offers a unique opportunity to isolate and study initial state radiation effects, as a kind of calibration standard. It is gratifying to note that good agreement is obtained between our model results and the experimental data. It is maybe less satisfying, but still informative, that the basic model can be varied in a number of ways without significantly changing the physics output. In other words, comparison with data is not likely to tell us e.g. whether k_T^2 rather than Q^2 is the proper evolution variable in the Altarelli-Parisi equations. This does not mean that there is no information to be had from a continued study of initial state radiation. On the contrary, much remains to be studied and understood, e.g. in the field of multijet production. Simple models of the kind we have presented here are going to prove invaluable in such studies, in establishing a well-defined baseline with respect to which non-trivial phenomena may be gauged.

Acknowledgements

One of us (T.S.) would like to acknowledge helpful conversations with T. D. Gottschalk, G. Marchesini and F. E. Paige.

References

1. UA1 Collaboration, G. Arnison et al., Lett. Nuovo Cimento 44 (1985) 1

2. UA2 Collaboration, J. A. Appel et al., CERN-EP/85-166

3. R. K. Ellis, D. A. Ross, A. E. Terrano, Nucl. Phys. B178 (1981) 421
   J. A. M. Vermaseren, K. J. F. Gaemers, S. J. Oldham, Nucl. Phys. B187 (1981) 301
   K. Fabricius, G. Kramer, G. Schierholz, I. Schmitt, Z. Physik C11 (1982) 315

4. G. C. Fox, S. Wolfram, Nucl. Phys. B168 (1980) 285
   R. Odorico, Nucl. Phys. B172 (1980) 141
   C.-H. Lai, J. L. Petersen, T. F. Walsh, Nucl. Phys. B173 (1980) 141
   T. D. Gottschalk, Nucl. Phys. B214 (1983) 201

5. K. Kajantie, E. Pietarinen, Phys. Lett. 93B (1980) 269

6. G. Marchesini, B. R. Webber, Nucl. Phys. B238 (1984) 1
   B. R. Webber, Nucl. Phys. B238 (1984) 492

7. T. Sjöstrand, LU TP 85-10, to be published in Computer Phys. Comm.

8. L. V. Gribov, E. M. Levin, M. G. Ryskin, Phys. Rep. 100 (1983) 1

9. A. Bassetto, M. Ciafaloni, G. Marchesini, Phys. Rep. 100 (1983) 202

10. R. Odorico, Nucl. Phys. B228 (1983) 381
    R. Odorico, Computer Phys. Comm. 32 (1984) 139

11. R. D. Field, G. C. Fox, R. L. Kelly, Phys. Lett. 119B (1982) 439
    M. P. Shatz, Caltech thesis/preprint CALT-68-1145 (1984)

12. T. Sjöstrand, Phys. Lett. 157B (1985) 321

13. T. D. Gottschalk, in Proc. of 1984 SSC Summer Study, Eds. R. Donaldson, J. G. Morfin, p. 78
    T. D. Gottschalk, Caltech preprint CALT-68-1241 (1985)

14. G. Altarelli, G. Parisi, Nucl. Phys. B126 (1977) 298

15. E. Eichten, I. Hinchliffe, K. Lane, C. Quigg, Rev. Mod. Phys. 56 (1984) 579

16. D. W. Duke, J. F. Owens, Phys. Rev. D30 (1984) 49

17. M. Glück, E. Hoffmann, E. Reya, Z. Physik C13 (1982) 119

18. F. A. Berends, R. Kleiss, Nucl. Phys. B260 (1985) 32

19. N. Mitra, Nucl. Phys. B218 (1983) 145

20. F. Halzen, D. M. Scott, Phys. Rev. D18 (1978) 3378

21. B. Andersson, G. Gustafson, G. Ingelman, T. Sjöstrand, Phys. Rep. 97 (1983) 33

22. H.-U. Bengtsson, Computer Phys. Comm. 31 (1984) 323

23. T. Sjöstrand, FERMILAB-Pub-85/119-T

24. H.-U. Bengtsson, G. Ingelman, Computer Phys. Comm. 34 (1985) 251
    H.-U. Bengtsson, T. Sjöstrand, in preparation

25. F. Halzen, A. D. Martin, D. M. Scott, M. P. Tuite, Z. Physik C14 (1982) 351

26. J. Owens, E. Reya, Phys. Rev. D17 (1978) 3003

27. G. Altarelli, R. K. Ellis, M. Greco, G. Martinelli, Nucl. Phys. B246 (1984) 12
    G. Altarelli, R. K. Ellis, G. Martinelli, Z. Physik C27 (1985) 617

28. C. T. H. Davies, B. R. Webber, W. J. Stirling, Nucl. Phys. B256 (1985) 413

29. R. Odorico, Phys. Rev. D31 (1985) 49

30. V. Barger, T. Gottschalk, J. Ohnemus, R. J. N. Phillips, Phys. Rev. D32 (1985) 2950

31. F. E. Paige, S. D. Protopopescu, Brookhaven preprint BNL-37271

32. UA1 Collaboration, G. Arnison et al., CERN-EP/85-116

33. UA1 Collaboration, G. Arnison et al., Phys. Lett. 132B (1983) 214

34. H.-U. Bengtsson, W.-S. Hou, A. Soni, D. H. Stork, Phys. Rev. Lett. 55 (1985) 2762

Table 1

Results for W production at 600 GeV with model variations, described in more detail in the main text.

no	model variations with respect to standard	$\langle p_{TW}\rangle$ for raw GeV	smear GeV	e sel GeV	associated jet properties 1jet %	2jet %	3jet %	4jet %	$\langle n_j\rangle$	$\langle p_{Tj}\rangle$ GeV
	UA1	-	-	7.3	29.	4.6	2.9	1.2	0.52	12.4
	UA2 (not same smearing)	-	-	8.5	-	-	-	-	0.29	17.8
1	standard values	6.7	7.4	7.0	25.	5.3	0.7	0.1	0.38	13.9
	.. without smearing				21.	3.0	0.3	0.	0.28	15.9
2	EHLQ2, Λ = 0.29	7.1	7.7	7.3	26.	6.3	0.9	0.1	0.42	13.8
3	DO2, Λ = 0.4	7.4	8.0	7.6	27.	6.4	1.1	0.1	0.44	13.8
4	coherent timelike showers	7.5	8.1	7.7	28.	6.4	0.7	0.0	0.43	14.1
5	no timelike showers	7.8	8.3	7.9	29.	6.0	0.6	0.0	0.43	14.7
6	no soft gluon summation	6.3	6.9	6.5	24.	4.9	0.7	0.1	0.37	13.3
7	$Q^2/4 \rightarrow Q^2$ in α_s etc.	5.8	6.5	6.2	22.	3.9	0.6	0.1	0.32	13.6
8	$Q^2/4 \rightarrow (1-z)Q^2$ in α_s	6.4	7.1	6.8	25.	5.7	0.8	0.1	0.39	13.6
9	evolution in $k_T^2 = (1-z)Q^2$	6.5	7.2	6.8	24.	5.2	0.5	0.1	0.37	13.6
10	ev. in k_T^2 + upper cut	6.3	7.0	6.7	25.	4.5	0.7	0.2	0.36	13.1
11	nonordered Q^2 allowed	6.4	7.0	6.7	25.	5.4	0.7	0.1	0.38	13.5
12	$Q^2_{max} = 9m_W^2/4$	7.2	7.8	7.5	27.	5.8	0.9	0.1	0.41	14.6
13	$Q^2_{max} = m_W^2/4$	5.3	6.0	5.9	23.	3.0	0.5	0.1	0.31	11.4
14	$Q^2_{min} = 1\ GeV^2$	6.6	7.3	6.9	24.	5.3	0.5	0.1	0.37	13.7
15	$Q^2_{min} = 16\ GeV^2$	6.5	7.2	6.8	25.	5.3	0.7	0.2	0.38	13.6
16	no primordial k_T	6.8	7.4	7.1	26.	5.8	0.6	0.1	0.40	14.0
17	no multiple interactions	6.7	7.2	6.9	22.	4.2	0.4	0.1	0.32	14.3
18	multiple interactions × 4	6.8	7.6	7.3	29.	6.7	1.0	0.1	0.46	13.8

Figure Captions

Fig. 1. The development of a spacelike shower.

a) A single initial parton is seen to branch into more and more partons as the Q^2 resolution scale is increased (moving rightward). A hard scattering, marked by a cross, selects a main chain of branchings, stronger lines.

b) Spacelike fluctuations on side branches must recombine, leaving a single sequence of branchings. Some partons may have a timelike virtuality, however, and give rise to associated timelike showers, shown dashed (with decreasing m^2 moving rightward).

Fig. 2. Schematic picture of a hard interaction between two partons 1 and 2, with preceding shower development. Partons 4, 6 and 8 may initiate timelike showers.

Fig. 3. The definition of what is the hard scattering rather than the initial state radiation may be ambiguous, see text.

Fig. 4. W transverse momentum spectra. Histograms give experimental data, UA1 [1] full and UA2 [2] dashed. Curves give model calculation results, the correct distribution dashed and after detector smearing etc. full.

Fig. 5. The fraction of events that contain at least one jet as a function of p_{TW}. Notation as in Fig. 4.

Fig. 6. The distribution in $\cos\theta^*$ (see text for exact definition of this polar angle) of jets in W events; crosses UA1 [1] data and full line model results.

Fig. 7. Transverse momentum distribution of Z^0 and associated transverse energy at 540 GeV, full our model results, dashed Halzen et al. [25].

Fig. 8. Transverse momentum distribution of centrally produced W, using DO1 structure functions. Full our model results, dashed Altarelli et al. [27], at CM energies 0.63, 1.6 and 10 TeV, from top to bottom.

Fig. 9. Transverse momentum distribution of W at 540 GeV, absolute normalization in number of events expected per 3 GeV. Dashed is result of Davies et al. [28] with DO1 and dotted with DO2 structure functions. For our results, an arbitrary K-factor of 2 has been introduced: dash-dotted with DO1 and full with DO2 structure functions.

Fig. 10. Distribution of $(1/\sigma)d\sigma/dp_{TW}^2 = (1/2\sigma p_{TW})d\sigma/dp_{TW}$ at CM energies 0.6 TeV full, at 2.0 TeV dashed, at 10 TeV dash-dotted and at 40 TeV dotted.

a) All rapidities.

b) Central production ($|y|\leq 0.5$).

Fig. 11. Particle distribution in azimuthal angle with respect to the W direction, in the transverse rest frame of hadrons, full for $4\leq p_{TW}\leq 8$, dashed for $8\leq p_{TW}\leq 12$ and dash-dotted for $p_{TW}\geq 12$ GeV.

Fig. 12. Distribution of $\langle -\bar{p}_{TW}\bar{p}_{Thad}\rangle/\langle p_{TW}^2\rangle$ as a function of azimuthal angle ϕ between W and hadrons (folded at $\pi/2$), dashed without and full with associated timelike showers.

Fig. 13. Jet cross-section at 540 GeV, dotted without initial or final state radiation, dash-dotted with initial state radiation but no final one and no associated timelike showers, dashed with both initial and final state radiation, full UA1 results [32].

Fig. 14. Jet profiles, i.e. energy flow per 0.05 units of pseudorapidity on the same side in azimuth as a jet trigger of given transverse energy, dotted 15 GeV, full 35 GeV and dashed 90 GeV, all for $s^{1/2}$ = 540 GeV. The distribution is symmetric in $\eta-\eta_{jet}$, so that only $\eta-\eta_{jet} > 0$ is shown.

a) Including initial and final state radiation.

b) Without initial or final state radiation.

Fig. 15. Jet profiles, defined as for Fig. 14, but with E_{Tmin} = 90 Gev fixed and with varying CM energy, full 540 GeV, dashed 2 TeV and dotted 10 TeV.

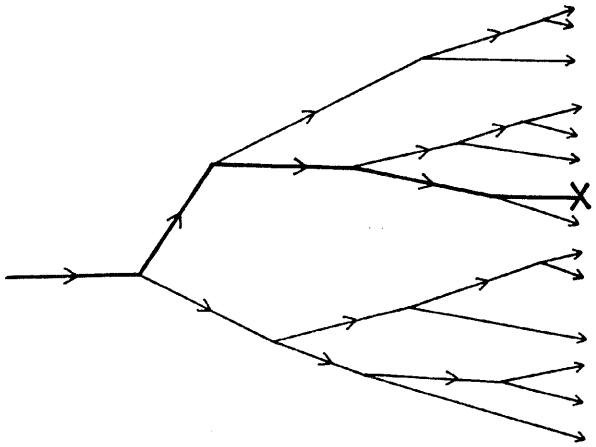

a

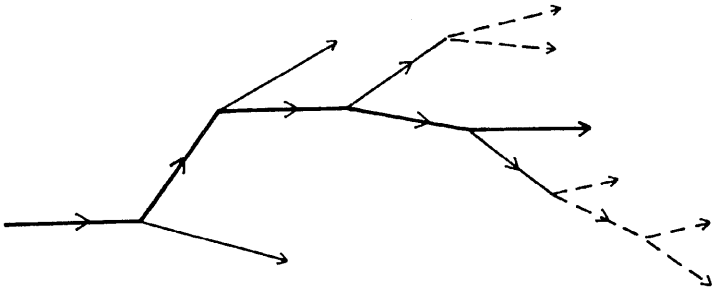

b

Fig. 1

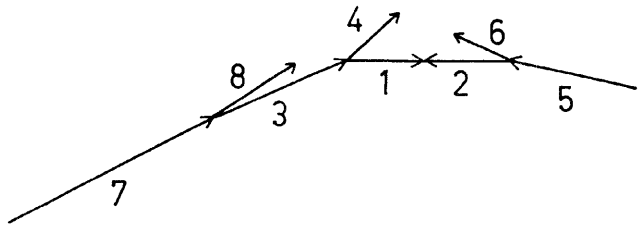

Fig. 2

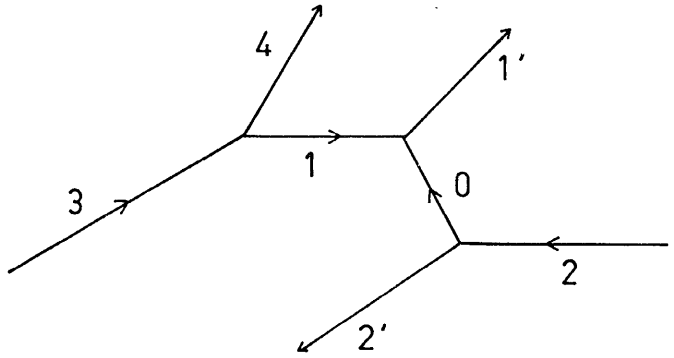

Fig. 3

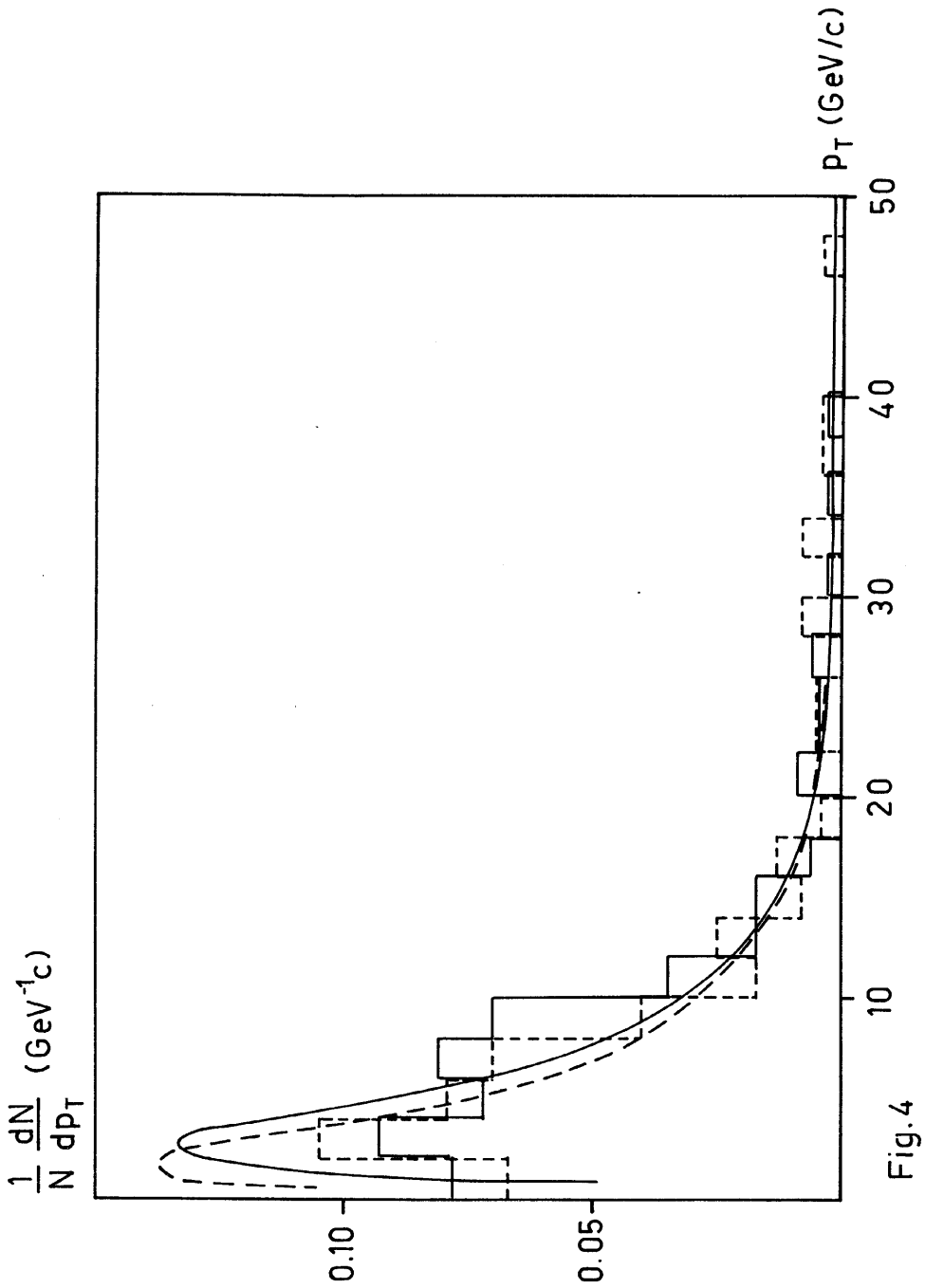
$\frac{1}{N}\frac{dN}{dp_T}$ (GeV^{-1}c)
0.10
0.05
10
20
30
40
50
p_T (GeV/c)

Fig.4

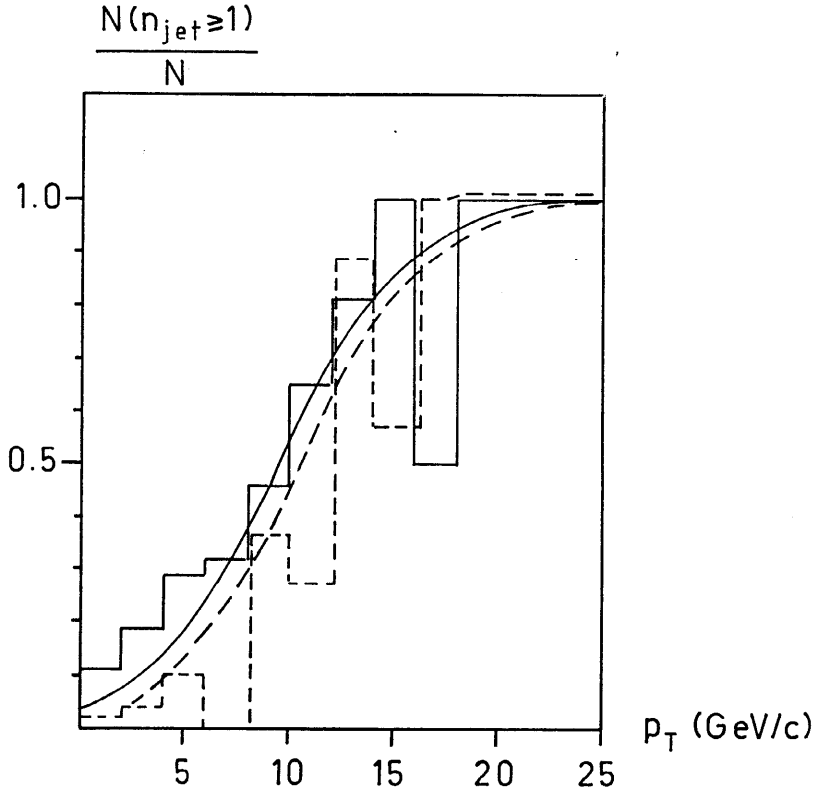
$\frac{N(n_{jet} \geq 1)}{N}$
1.0
0.5
5
10
15
20
25
p_T (GeV/c)

Fig.5

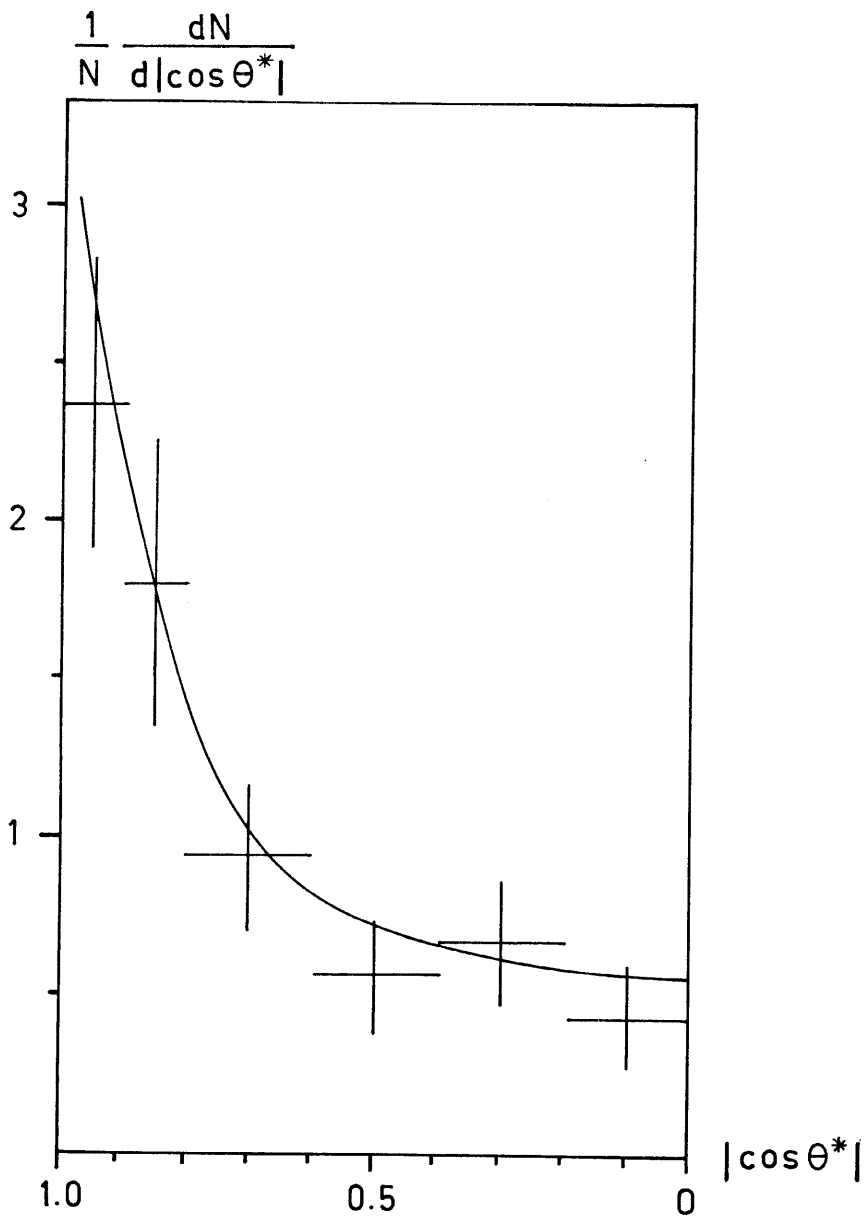
$\frac{1}{N}\frac{dN}{d|\cos\theta^*|}$
3
2
1
1.0
0.5
0
$|\cos\theta^*|$

Fig. 6

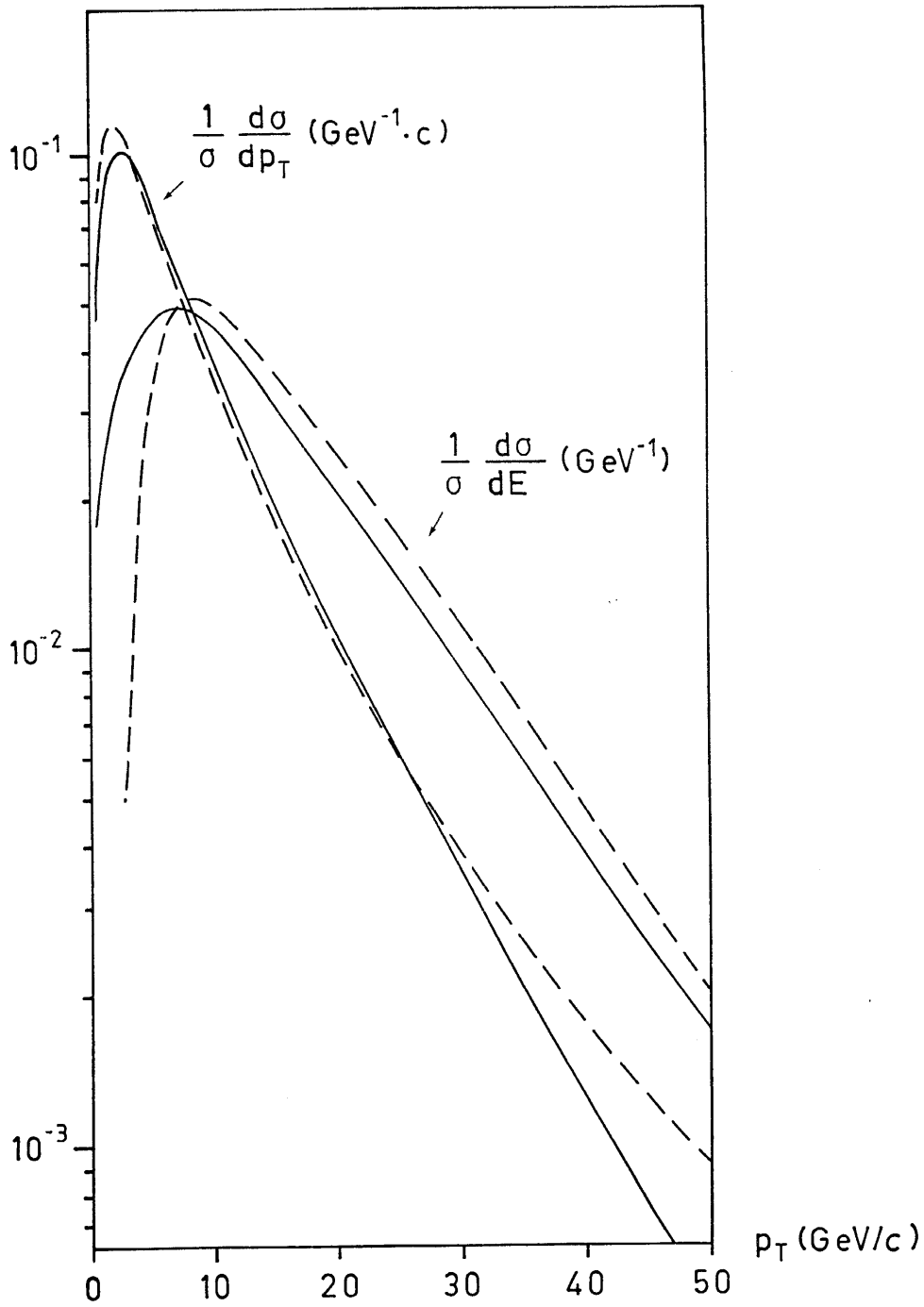
$\frac{1}{\sigma}\frac{d\sigma}{dp_T}$ (GeV^{-1}·c)
$\frac{1}{\sigma}\frac{d\sigma}{dE}$ (GeV^{-1})
10^{-1}
10^{-2}
10^{-3}
0
10
20
30
40
50
p_T (GeV/c)

Fig. 7

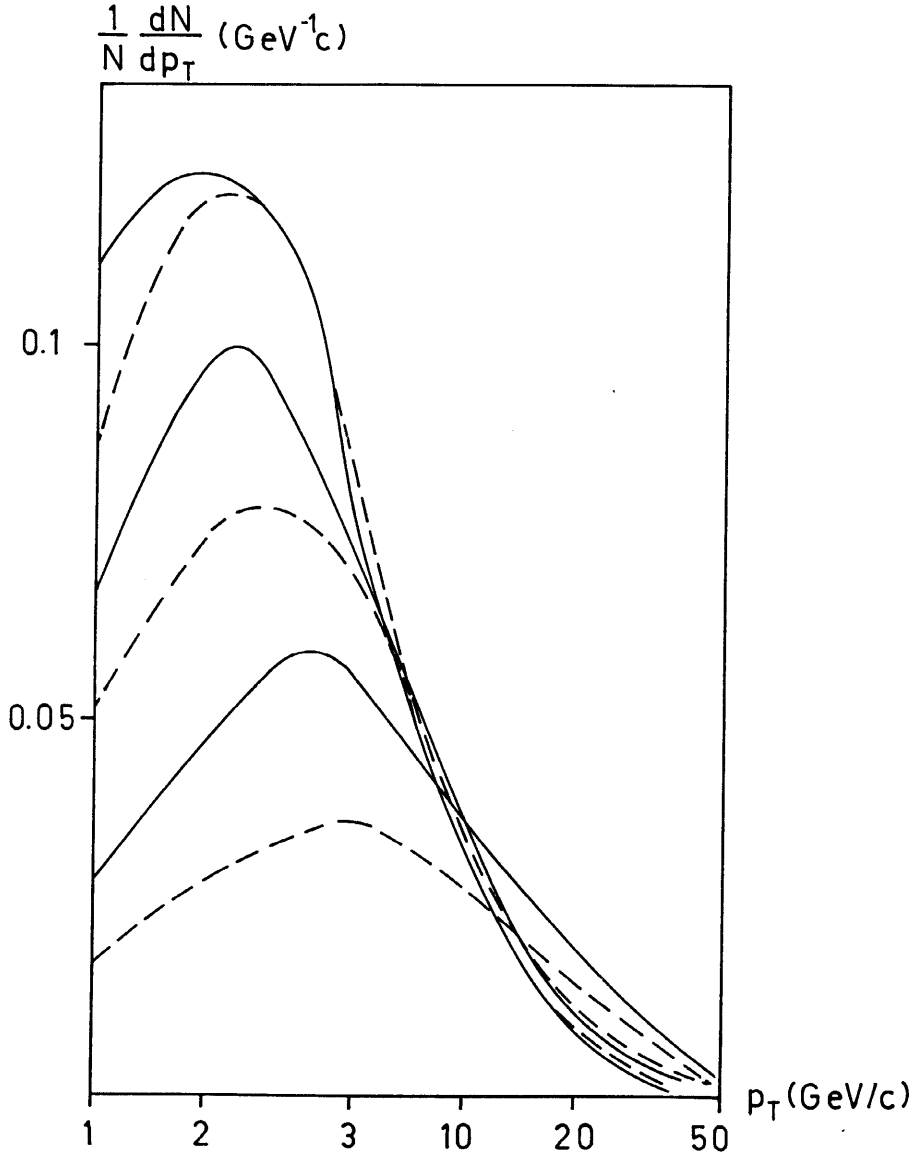
$\frac{1}{N}\frac{dN}{dp_T}$ (GeV^{-1}c)
0.1
0.05
1
2
3
10
20
50
p_T(GeV/c)

Fig.8

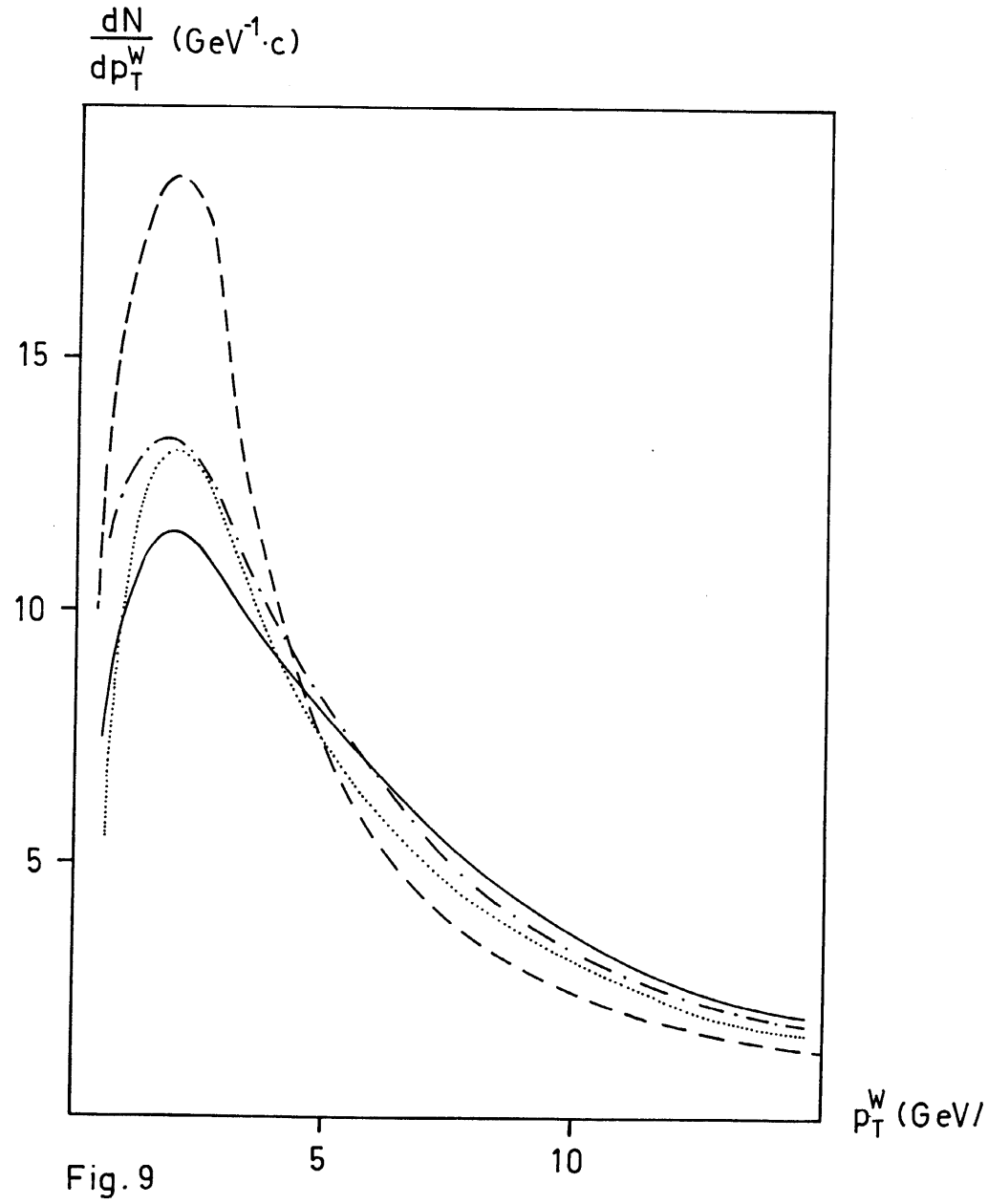
$\frac{dN}{dp_T^W}$ (GeV^{-1}·c)
15
10
5
5
10
p_T^W (GeV/

Fig. 9

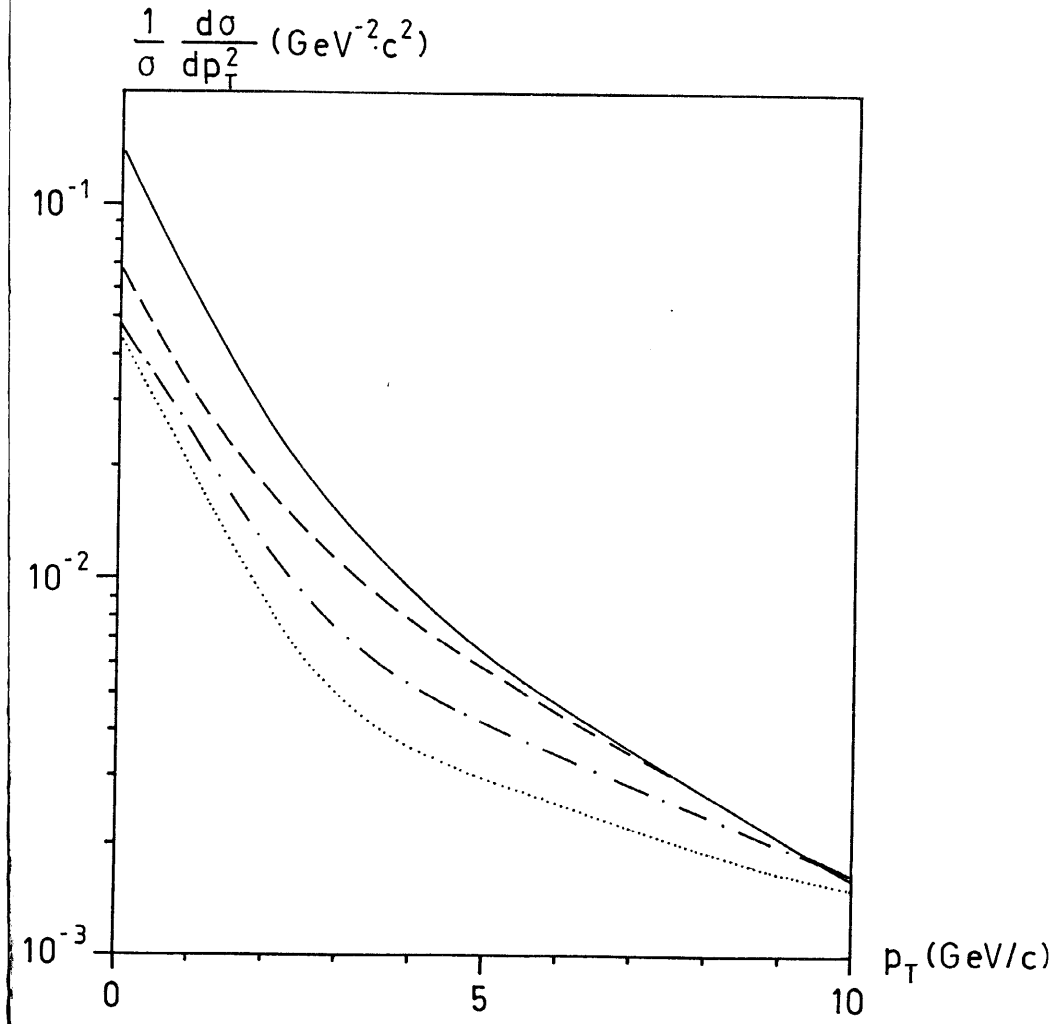

Fig. 10 a

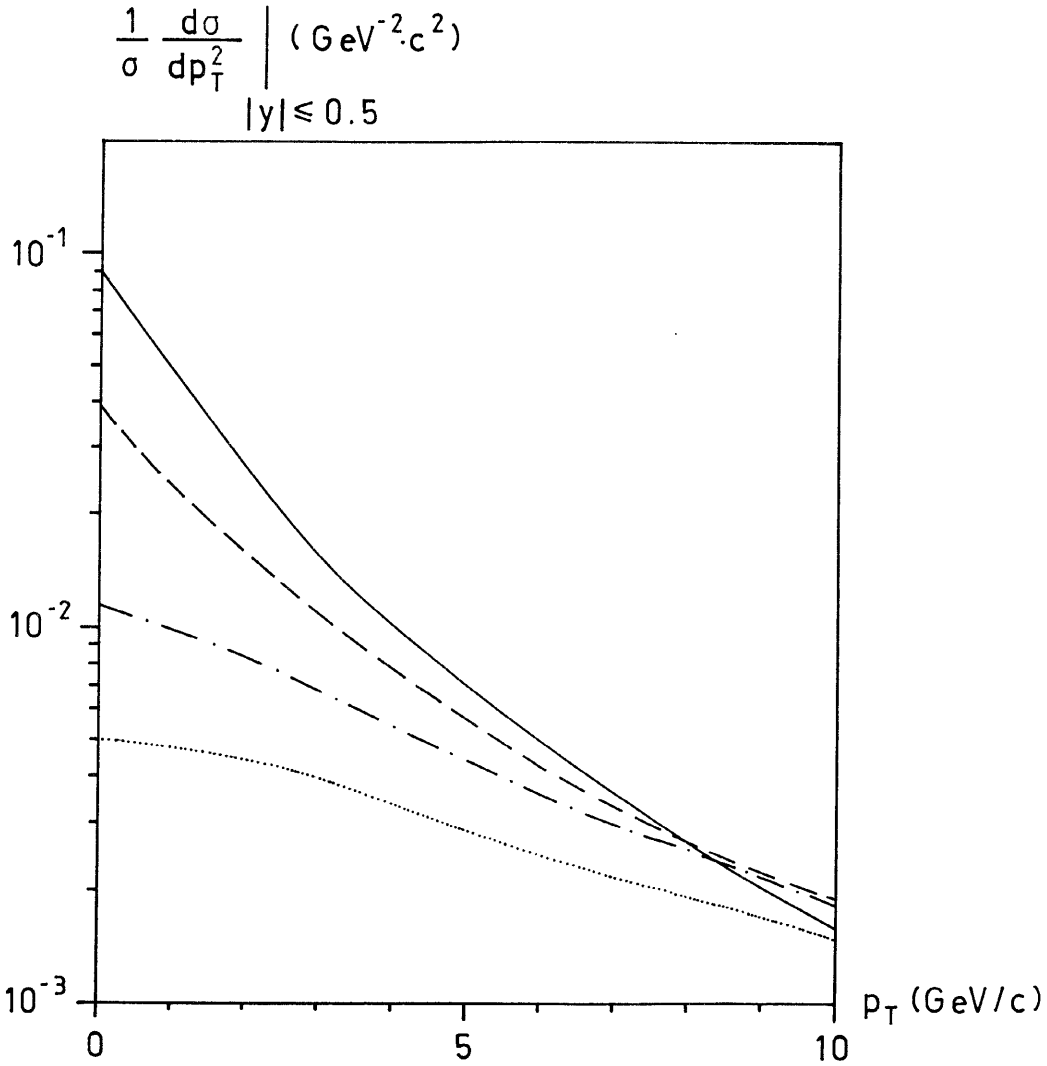

Fig. 10 b

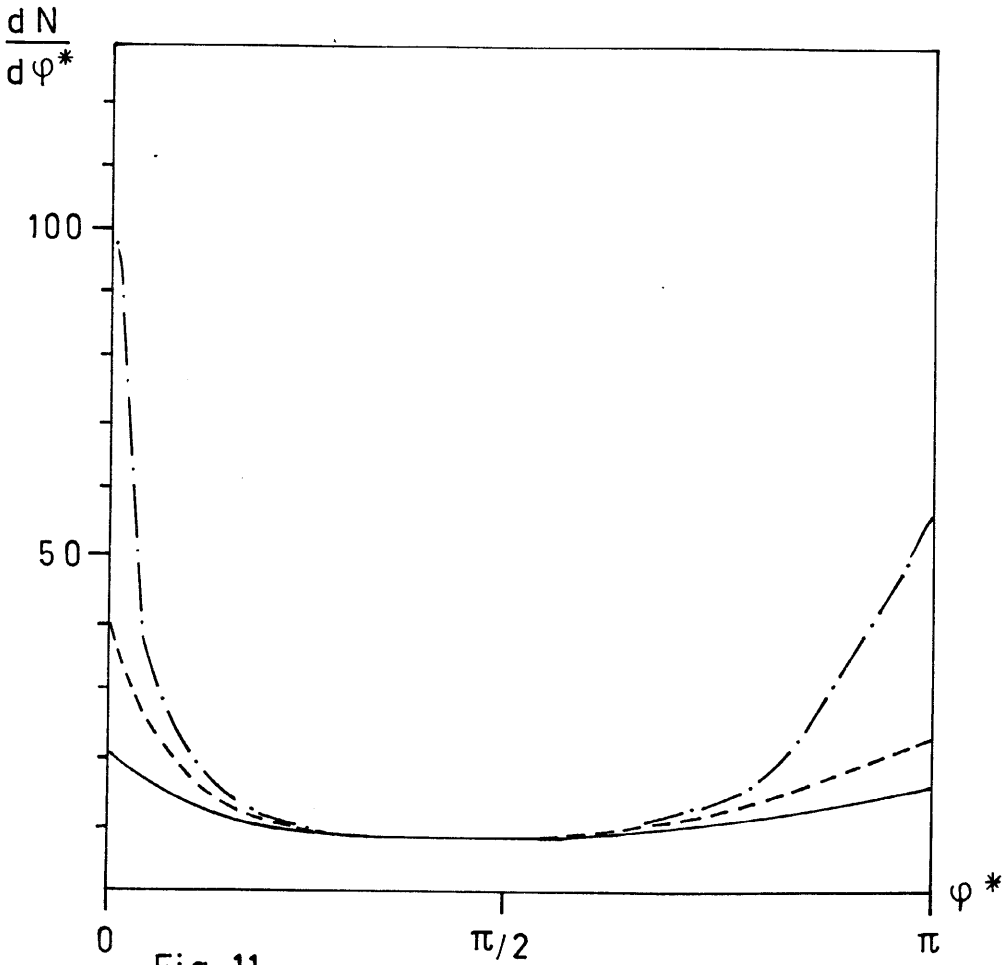

Fig. 11

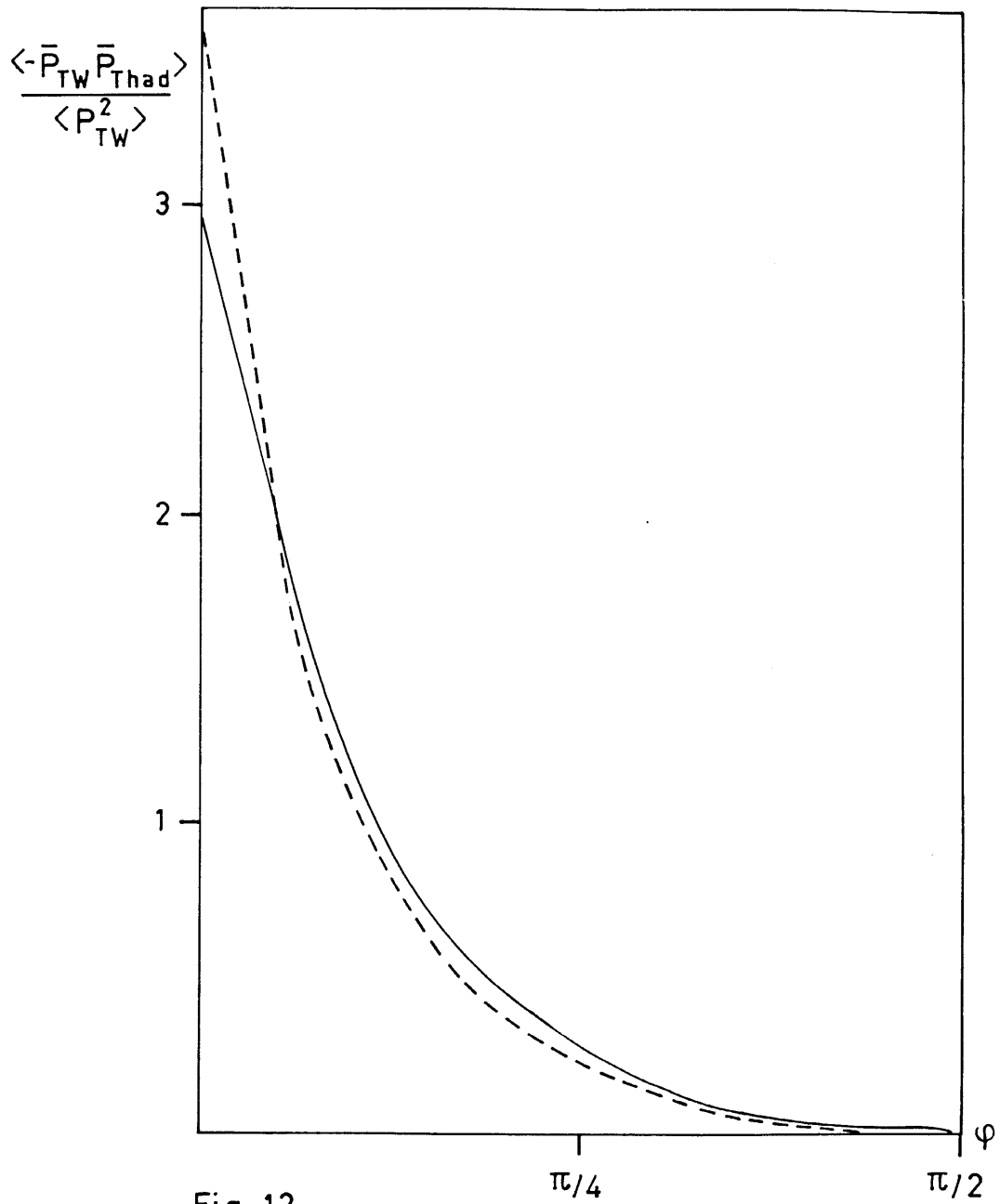

Fig. 12

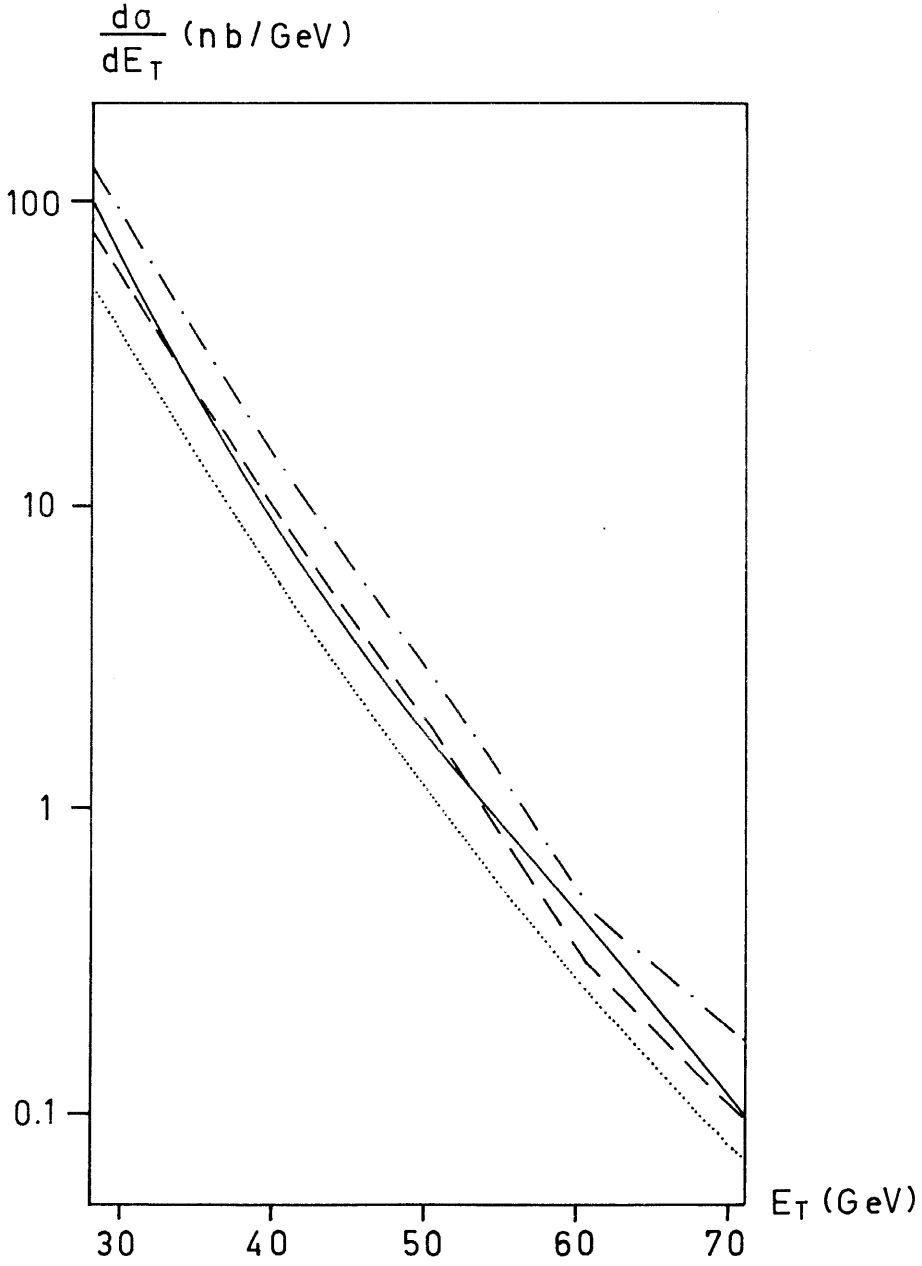

Fig.13

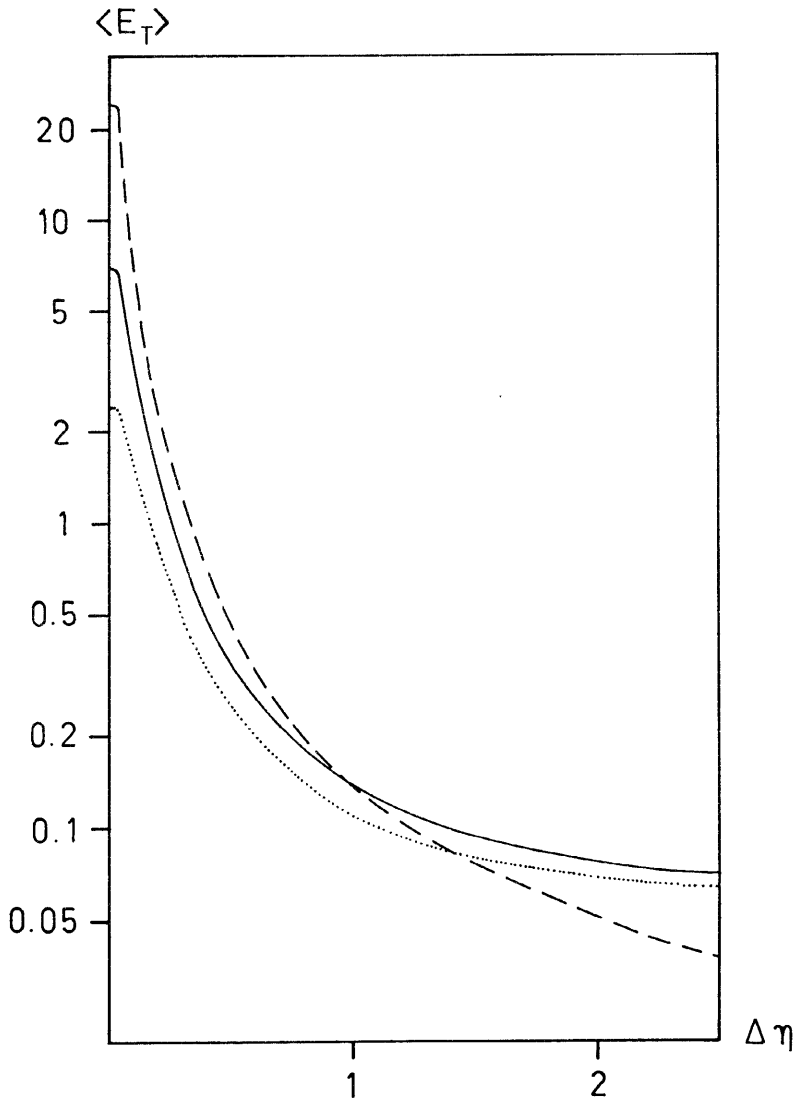

Fig. 14 a

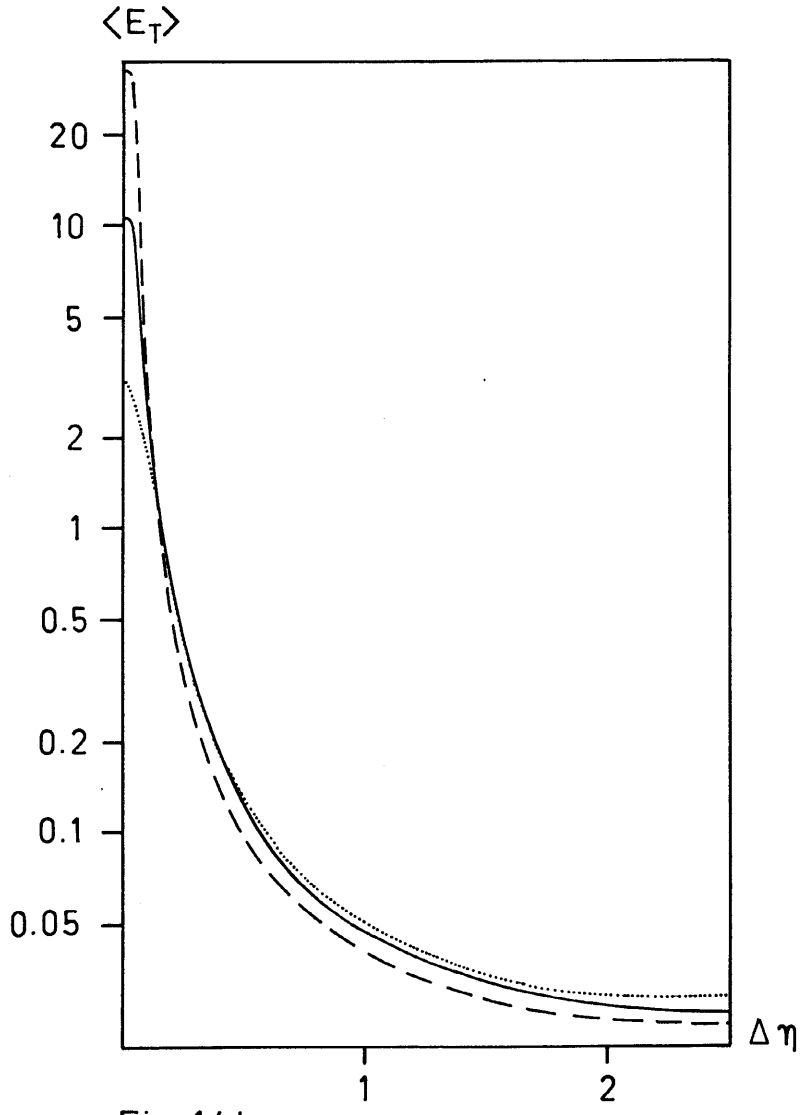

Fig. 14 b

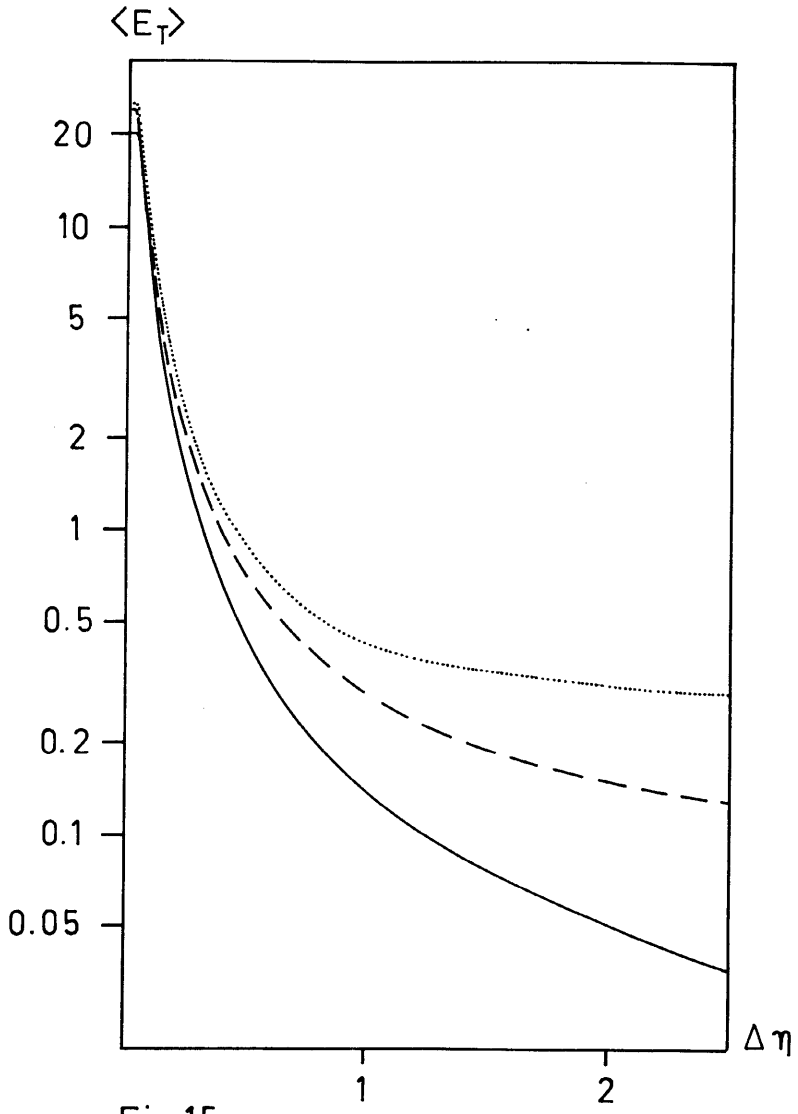

Fig.15